In silico identification of potential *Pv*FKBP35 inhibitors from *Entadrophragma angolense* Limonoids extracts as antimalarial agents

Latif Adams [a,f,*], Abdul Rashid Issahaku [b,c], Clement Agoni [b,c], Michael Afiadenyo [d], Kwadwo Asamoah Kusi [e], Siobhan Moane [a], Dorcas Obiri -Yeboah [f], Michelle McKeon-Bennett [a,**]

[a] Technological University of Shannon: Midlands Midwest, Midlands Campus, Athlone, Ireland
[b] Discipline of Pharmaceutical Sciences, School of Health Sciences, University of KwaZulu-Natal, Westville Campus, Durban, 4001, South Africa
[c] West African Centre for Computational Research and Innovation, Ghana
[d] Department of Parasitology, Noguchi Memorial Institute for Medical Research (NMIMR), College of Health Sciences (CHS), University of Ghana, Legon, Accra, Ghana
[e] Department of Immunology, Noguchi Memorial Institute for Medical Research (NMIMR), College of Health Sciences (CHS), University of Ghana, Legon, Accra, Ghana
[f] Department of Microbiology and Immunology, School of Medical Sciences, College of Health and Allied Sciences, University of Cape Coast, Cape Coast, Ghana

ARTICLE INFO

ABSTRACT

Plasmodium species, which are spread by female *Anopheles* mosquitoes, are responsible for malaria. Out of the five major *Plasmodium* species, *Plasmodium falciparum* and *Plasmodium vivax* are the most deadly and invasive species responsible for 99.7% and 75% of malaria cases in Africa and America respectively. Despite the invasive nature of malaria, the *Plasmodium* parasite continues to develop resistance to current drugs. It is therefore imperative to come up with new therapeutics to combat malaria. Previous studies have reported that Limonoids from the *Meliaceae* family possess antimalarial properties. This study therefore aims at employing computational approaches to identify potential antimalarial Limonoids by targeting *Pv*FKBP35. *Pv*FKBP35 has been reported to be a suitable target for antimalarial therapeutics as it is involved in various physiological activities including transcription, protein stability and folding. Molecular docking, Molecular Dynamics simulation and Molecular Mechanics-Poisson Boltzmann Surface Area calculation were employed to identify the potential leads. Sixteen [16] Limonoids extracted from the bark of the stem of *Entadrophragma angolense* were virtually screened against *Pv*FKPB35. The top hit compounds were subjected to 500 ns Molecular Dynamics simulation and Molecular Mechanics – Poisson Boltzmann Surface Area calculations to examine their stability and free binding energy. Two potential leads, compounds **1** and **11** with binding energies −6.3 and −5.4 kcal/mol respectively were identified. The potential leads in complexed with *Pv*FKBP35 had an average root mean square deviation of 1.18 ± 0.19 Å and 3.12 ± 0.60 Å, indicating their stability. Solvent Accessible Surface Area was utilized to predict the penetrative ability of the compounds into the binding pocket. Average Solvent Accessible Surface Area values of 327.88 ± 47.54 Å^2, 402.18 ± 39.81 Å^2 were obtained for compounds **1** and **11** respectively. ADMET estimations of compounds **1** and **11** predicted them to be druglike and do not violate Lipinski's rule of five. Compounds **1** and **11** need be tested *in vitro* to validate their antimalarial activity although they were predicted to be antiprotozoal with Pa values 0.207 and 0.162. These compounds can then serve as the scaffold for the design of novel antimalarial therapeutics.

1. Introduction

Malaria is a life-threatening tropical disease, caused by *Plasmodium* species, transmitted by the female *Anopheles* mosquitoes affecting millions of people worldwide [1]. According to the latest World Malaria Report, there were 247 million cases and 619,000 deaths recorded in 2021(1). Africa alone accounts for 95% of malaria cases and 96% of death, with 80% of fatalities occurring in children under 5 years old [2]. Other risk groups include pregnant women, immunocompromised patients, and travelers [2].

* Corresponding author. Technological University of Shannon: Midlands Midwest, Midlands Campus, University Road, Athlone, Co. Westmeath, Ireland.
** Corresponding author. Technological University of Shannon: Midlands Midwest, Midlands Campus, University Road, Athlone, Co. Westmeath, Ireland.
E-mail addresses: latifadams2016@yahoo.com, abdullatif.adams@tus.ie (L. Adams), michelle.mckeonbennett@tus.ie (M. McKeon-Bennett).

Malaria is caused by five major species: *Plasmodium falciparum, Plasmodium malariae, Plasmodium knowlesi, Plasmodium ovale*, and *Plasmodium vivax* [3,4]. Amongst, these both *P. falciparum* and *P. vivax* are the most dangerous and prevalent species [1,5]. *P. falciparum* is responsible for the majority of malaria cases and deaths, *P. vivax* causes significant morbidity, particularly in South America and the Asia-Pacific region [2,6].

According to the world malaria report 2021, *P. falciparum* accounted for more than 90% of estimated malaria cases in the World Health Organization (WHO) African Region, 50% of cases in the WHO South-East Asia Region, 71% of cases in the Eastern Mediterranean, and 65% in the Western Pacific. On the other hand, *P. vivax* was the predominant parasite in the WHO Region of the Americas, representing 75% of malaria cases [1,2,7].

While less prevalent*, P. malariae* and *P. ovale* are found in endemic regions particularly in sub-Saharan Africa [8,9] Additionally, cases of *P. knowlesii* infection have also been reported from the forested regions of South-East Asia [10–12].

The clinical manifestation of Malaria is divided into two forms: uncomplicated and severe malaria. Early signs and symptoms of uncomplicated malaria include fever, chills, headache, muscle pains, cough, vomiting, and diarrhea [13]. On the other hand, severe malaria presents more serious symptoms, such as severe anemia, cerebral malaria, acute lung injury, respiratory distress, and multiple organ failures [14–16].

The current chemotherapies approved for the treatment of Malaria and recommend by the WHO include chloroquine and artemisinin-based combination therapies (ACTs) and their derivatives [17]. These treatments work by targeting crucial biological molecules involved in various biological process of malaria parasites. Chloroquine targets the action of heme polymerase in *Plasmodium* species, causing a toxic buildup of heme and eventually killing the parasite [18]. On the otherhand, artemisinin targets the enzyme proteasome, causing protein damage, and effectively, killing the malaria parasite [19,20].

However,. there are reports on the development of resistance to current drugs by the malaria parasites [21–26] and have spread to many malaria endemic regions [17,25,27,28]. The emergence and widespread distribution of multi-drug resistant strains of Plasmodium pose a major challenge to malaria control, thus resulting in high morbidity and mortality [23], This situation underscores the urgent need for the development of new alternative effective antimalarial agents to combat menace.

Natural products such as medicinal plants remain one of the potential source for the development of new effective antimalarial drugs [29, 30]. Two modern antimalarial drugs, quinine and artemisinin were extracted and isolated from medicinal plants [31]. Medicinal plants contain bioactive compounds effective against several diseases and ailments including, life-threatening ones such as malaria [32–35]. Notably, the WHO, reports that approximately about 80% of developing countries depend on medicinal plants for their primary health care needs [36,37]. These plants are cost-effective, readily available, and easily accessible with few side effects compared to orthodox drugs [38] and making them viable alternatives for the development of new therapeutic agents.

Entadrophragma angolense (Meliaceae), known as "the mahogany tree", widely distributed in tropical Africa and used in traditional medicine to treat several diseases. The stem bark is reported to treat gastrointestinal disorders such as peptic ulcer in humans, fever, wounds, cancer, rheumatism, eye infections, and malaria [39] Phytochemical investigation of *E. angolense* have revealed the presence of limonoids, triterpenoids steroids, and fatty acids and phenolic compounds [40]. Pharmacological studies of this plant have demonstrated antimicrobial [41], antifeedant [42], antiulcer [43], antioxidant [44], anti-inflammatory [45,46] and antimalarial properties [47]. In west Africa, *E. angolense* is ethnomedicinally used to treat malaria [48,49]. Studies have also reported the isolation of novel limonoids (7α-obacunyl acetate and cycloartane) from the stem bark of *E. angolense* with potent anti-plasmodial activities [47].

Limonoids are essential and abundant bioactive compounds found in the family *Meliaceace* exhibiting several biological properties [50,51]. In a study by Zhang et al. 2016, 16 new limonoids entangolensins A-P (Table 1) were isolated from the stem barks of *E. angolense* [52]. Bioactivity screening in their report further revealed that compounds 6, 12, 15 and 17 showed moderate cytotoxicity against HepG2 and MCF-7 cell lines, with IC$_{50}$ values from 13.19 to 36.93 μM; Additionally, compound 6, 11 and 17 exhibited significant inhibitory activity against Nitric Oxide (NO) in LPS-activated RAW 264.7 macrophages, with IC$_{50}$ values of 1.75, 7.94 and 4.63 μM respectively [52].

Having been reported to possess possible antimalarial properties particularly in the study by Amoa Onguéné et al. we sought to further explore their finding using molecular modelling techniques against *Pv*FKBP35, an experimentally reported therapeutic targets in the treatment of malaria. As a member of the immunophilin family, *Pv*FKBP35 is known to exhibit a canonical peptidyl-prolyl *cis*-trans isomerase (PPIase) or rotamase activity and regulate various physiological functions including protein stability and folding [53–55], neuroprotective and neurotrophic activities [56], protein trafficking [57,58], receptor signaling [59–61], calcium homeostasis [59,62], transcription [63], spermatogenesis [64] and histone chaperone activity [65,66]. *Pv*FKBP35 is thus an crucial enzyme in the parasite's growth [67–71] thereby making it a potential drug target [72,73]. The therapeutic modulation of *Pv*FKBP35 is furthers established in the report by Harikishore et al. where the therapeutic modulation of PvFKBP35 was shown by a co-crystallization with a potential binder, D5I (N'-(1-adamantylcarbonyl) pyridine-4-carbohydrazide [74].

In this report, we employ computational techniques to explore the therapeutic potential of limonoids as lead molecules that could therapeutically modulate FK506 binding domains (FKBDs) of *Pv*FKBP35, towards the development of novel antimalarial agents. Computational methods in drug discovery accelerate drug discovery process and provide preliminary insights that can inform a drug discovery process [75–77]. The application of these methods for the drug discovery against neglected tropical diseases has also gained prominence in recent years with several reports incorporating these techniques [78–80]. Selected limonoids will be screened against *Pv*FKBP35 to identify the potential therapeutic modulators. By comparing, the binding dynamics of known therapeutic modulators of *Pv*FKBP35 as a control, findings from this report would also provide structural perspectives that could guide the experimental exploration of limonoids as antimalarial agents.

2. Computational methodology

2.1. PfFKBP35 structure preparation

The X-ray crystal structure of *Pv*FKBP35 co-crystallized with the

Table 1
Limonoids compounds isolated from stem bark of *Entandrophragma angolense*.

No.	Compound name	Source/reference
1	Entangolensin A	*E.angolense* [78]
2	Entangolensin B	*E.angolense* [78]
3	Entangolensin C	*E.angolense* [78]
4	Entangolensin D	*E.angolense* [78]
5	Entangolensin E	*E.angolense* [78]
6	Entangolensin F	*E.angolense* [78]
7	Entangolensin G	*E.angolense* [78]
8	Entangolensin H	*E.angolense* [78]
9	Entangolensin I	*E.angolense* [78]
10	Entangolensin J	*E.angolense* [78]
11	Entangolensin K	*E.angolense* [78]
12	Entangolensin L	*E.angolense* [78]
13	Entangolensin M	*E.angolense* [78]
14	Entangolensin N	*E.angolense* [78]
15	Entangolensin O	*E.angolense* [78]
16	Entangolensin P	*E.angolense* [78]

known binder D5I (N'-(1-adamantylcarbonyl) pyridine-4-carbohydrazide) was retrieved from the Protein Data Bank (PDB) [81] with PDB ID 4MGV. With D5I bound to the inhibitor binding domain of *Pv*FKBP35, its position was used as the binding site of the compounds to be explored. To reduce computational cost, only chain A was used in this study while all other non-standard co-crystallized residues on the PDB structure were also removed. Also, chain A contains the catalytic pocket of *Pv*FKBP35. In preparation for molecular docking and Molecular Dynamics (MD) simulations hydrogen atoms were removed and added respectively using UCSF Chimera 1.16 [82,83].

2.2. Preparation of investigated Limonoids

The limonoids investigated in this report were retrieved from a previous study [84]. The 2D structures of the 16 limonoids were then generated by sketching them with Marvin sketch 6.2.2 [85]. The sketched structured were then saved in spatial data file (SDF) format. Sketched 2D structures of the ligands were then converted to their respective 3D conformers using Avogadro 1.2.0 [86]. The energy of the 3D structures generated were subsequently minimized using the Universal Force Field (UFF) incorporated in the Avogadro which also optimizes the molecular geometries of the compounds with the steepest descent algorithm for structural minimization. The optimized and energy minimized structures were then saved in "mol2" format. In preparation for molecular docking, hydrogen atoms were removed from each ligand, appropriate Gasteiger charges were added and the "pdbqt" formats of all the ligands were then generated using AutoDock Vina [87]. Ligands selected for MD simulation were also prepared by adding hydrogen atoms, adding appropriate semi-empirical (AM1) with bond charge correction (BCC) charges, and subsequently saving structures in "mol2" formats [88,89].

2.3. Identification of binding site(s) and molecular docking

Molecular docking to predict the binding potential of the investigated limonoids towards with *Pv*FKBP35 was performed using AutoDock Vina v.1.2.0 as reported in our previous reports [78,90,91] A grid box around the binding site was generated with coordinates of x = 31.93, y = 35.61 and z = 29.25 (center dimensions) and x = 7.95, y = 9.89 and z = 12.21 Å (size dimensions) was generated. Molecular docking was performed using an exhaustiveness of 8 and the spacing was set at 1 Å. The output of molecular docking was viewed with UCSF Chimera using the integrated ViewDock module after which docked complexes were saved for further analysis.

2.4. Molecular Dynamic simulations

Molecular Dynamic (MD) simulations reveal imperative information pertaining to the biological systems dynamic evolution by exploration of the physical motion that occurs between molecules and atoms [92–95]. MD simulations for *Pv*FKBP35 complexed with the selected limonoids were subject to 500 ns MD simulations using the GPU version of AMBER 20 package [96]. The General Amber Force Field (GAFF) incorporated in the ANTECHAMBER module was employed to apply atomic partial charge to the selected limonoids [97,98]. The AMBER 20 LEAP module was employed for protein optimization and solvation for each system the systems. In all, three systems were constructed for the simulations; unbound *Pv*FKBP35, *Pv*FKBP35 complexed with the top two scoring docked limonoids and *Pv*FKBP35 complexed with the known binder, D5I. Each system was partially minimized for 2500 steps with a restraint potential of 500 kcal/mol. Thereafter, full minimization of 1000 steps were conducted in the absence of all restraints by conjugate gradient algorithm. The systems then underwent gradual heating from 0 to 300 K for 50ps to ensure each simulated system maintained a fixed number of atoms and volume. Each system was also subjected to a potential harmonic restraint of 10 kcal/mol with a collision frequency of 1 ps prior to

being equilibrated for 500 ps at 300 K. The atmospheric pressure was maintained at 1 bar by employing Berendsen barostat [99], thus enabling the pressure and number of atoms within each system to be constant, emulating an isobaric-isothermal ensemble (NPT). This procedure was followed by an MD simulation of 500 ns for each system, integrating the SHAKE algorithm to constrict the hydrogen atom bonds [100]. Each simulation had a step size of 2 fs, thus incorporating the single precision fixed point (SPFP) precision model. All simulations concurred with a constant pressure and temperature of 1 bar and 300 K respectively: a Langevin thermostat with a collision frequency of 1 ps randomized seedling, an isobaric-isothermal ensemble (NPT), and a pressure-coupling constant of 2 ps [94].

2.5. Post-dynamic analyses

After every 1 ps, the bound complexes and free enzyme coordinates were saved and their subsequent trajectories analyzed by the integrated CPPTRAJ module of the AMBER 20 package [101]. The thermodynamic energy of each system, together with the root mean square fluctuations (RMSF) of individual resides and root mean square deviation (RMSD) of the C-α atoms were examined. Graphical analysis and plots were generated using Microcal Origin 6.0 [102,103].

2.6. Binding free energy calculations

The Molecular Mechanics/Poisson Boltzmann Surface Area (MM/PBSA) approach [104,105] was used in this study to estimate the binding energies of the simulated complexes [92,94,106–110]. ([94, 110–113]. Although 300,000 frames were generated for each complexed system over the 300ns simulation period, in calculating the binding energies, only frames from the last 200 ns s were selected, ensuring only well equilibrated framed were considered MM/PBSA enables the prediction of binding free energies that are involved in complex formation providing insights into the binding affinity of each ligand to *Pv*FKBP35 Mathematically, the binding free energy (ΔG) for each complex is computed as follows:

$$\Delta G_{bind} = G_{complex} - (G_{receptor} + G_{ligand}) \tag{1}$$

$$\Delta G_{bind} = \Delta G_{gas} + \Delta G_{sol} - T\Delta S = \Delta H - T\Delta S \tag{2}$$

$$\Delta G_{gas} = \Delta E_{int} + {}_{\Delta}Eele + \Delta E_{vdW} \tag{3}$$

$$\Delta G_{sol} = \Delta G_{ele,sol(PB)} - \Delta G_{np,sol} \tag{4}$$

$$\Delta G_{np,sol} = \gamma SASA + \beta \tag{5}$$

The energy of the gas phase is depicted by ΔG_{gas}, defined as the summation of the internal (ΔE_{int}), electrostatic ($\Delta Eele$) and van der Waals (ΔE_{vdW}) energies. ΔGsol depicts the solvation free energy, and comprises of polar and nonpolar contribution states, ΔGele, sol and ΔGnp,sol; respectively. By estimation of the Poisson-Boltzmann (PB) ($\Delta Gele,sol(PB)$) model using the MM/PBSA method, the ($\Delta G_{ele,sol}$) was able to be derived, whilst ($\Delta G_{np,sol}$) was determined by employing equation (5), where the surface tension proportionality constant "γ" is set to 0.0072 kcal/(mol-1. $Å^{-2}$) with β being a constant. The solvent accessible surface area (SASA) ($Å^2$) is calculated by employing a linear incorporation of pairwise overlaps (LCPO) model. SASA, which depicts the solvent accessible surface area ($Å^2$) is calculated using a linear incorporation of pairwise overlaps (LCPO) model. The energy contribution of the essential residues of the active site gives us an indication of the role it plays in stabilizing the ligand within the binding pocket and the differential binding estimates by employing the integral per-residue decomposition analysis of MM/PBSA. Energy calculations were performed using the last xtc file which consisted of all the frames from the MD simulation and the reported energy values are the average of all the frames [94,95,114,115].

2.7. In silico prediction of the pharmacokinetics and physicochemical properties

Prediction of the pharmacokinetics of the investigated compounds were performed using the online-based prediction tool, Swiss ADME [116]. Parameters such as bioavailability score, blood-brain barrier permeability, gastro-intestinal absorption, hydrogen bond donors and acceptors, lipophilicity, molecular weight, synthetic accessibility, and water-solubility were subsequently computed [94]. The ProTox website server [117] was also used to determine the LD_{50} and oral toxicity of the investigated compounds.

2.8. PASS prediction

Prediction of Activity Spectra of Substances (PASS) was used to explore the biological properties of the potential leads. PASS is an online tool that is used to predict biological activities of compounds based on its chemical structure (http://www.way2drug.com/passonline/) [78, 118].
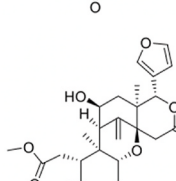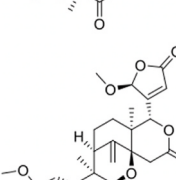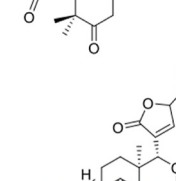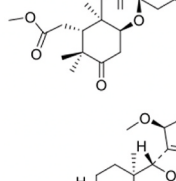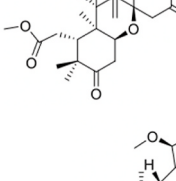
3. Results and discussion
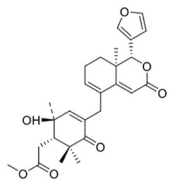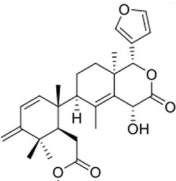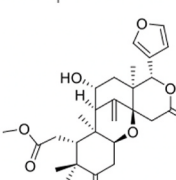
Targeting FK506-binding proteins (FKBP) has becomes an attractive escape route for malaria resistance [71,119]. This is a conserved region across the plasmodium genus [120–122], thus its inhibition has the potential to treat pan-parasitic infection. Since proteins are sensitive to stimuli, the binding of a small molecule to a target protein has the propensity to elicit responses which is initiated at the molecular level [123,124]. Therefore, we explored the structural dynamics of the binding of identified compounds to PvFKBP35 juxtaposing with the co-crystallized compound.

This was achieved by determining the stability of the compounds, their level of penetration into the hydrophobic core, and their motions along the principal component's axis. This investigations on the compounds' behavior were then accompanied by investigations of the structural dynamics of FKBP which is conditioned by these compounds' ligation. As such for the protein, the stability of the global protein, flexibility and compactness was determined by computing the changes in the C-α atoms. The solvent accessibility surface area of the protein which is informative on the folding and unfolding of the protein was also determined. This approach has been successfully employed by other investigations [125–127].
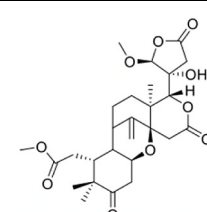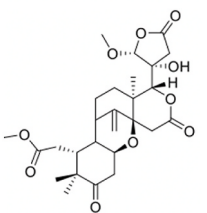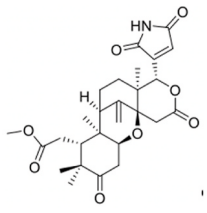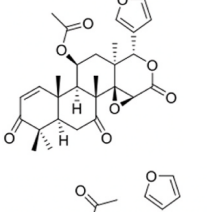
3.1. Molecular docking
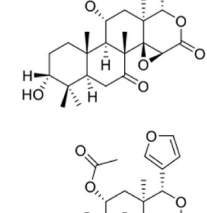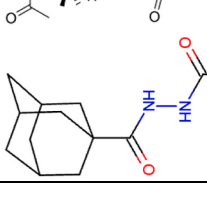
To determine the binding potential of the investigated limonoids towards FK506-binding proteins, each compound was individually docked into the resolved binding pocket occupied by D51 using Auto-Dock Vina. The co-crystallized D51 in complex with *Pv*FKBP35 by Harikishore et al. in 2013 [74] was used to map-out the binding region of the limonoids on *Pv*FKBP35. Residues of *Pv*FKBP35 that comprised the binding pocket included Tyr43, Phe54, Asp55, Phe64, Glu72, Val73, Ile74, Trp77, Tyr100, Cys105 and Phe117. Using the scoring function of Auto Dock Vina, the docking which corresponded with the stability of docked ligands was calculated and presented in Table 2. The experimentally reported binder, D5I was redocked into its pockets as control. As shown in Table 2, compound **1** showed the highest docking score of −6.3 kcal/mol amongst the limonoids suggesting it was the most stable with the D5I binding site on *Pv*FKBP35. Based on the docking scores, compound **1** was shown to exhibit superior stability within the binding region relative to D5I, the experimentally reported binder. The next favourably bound limonoid was compound **11** which showed a docking score of −5.4 kcal/mol. The docked complexes of compound **1**, compound **11** and D5I were then subjected to 500ns MD simulation to further explore the possible structural binding potential of the limonoids towards *Pv*FKBP35.
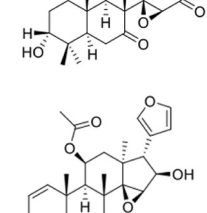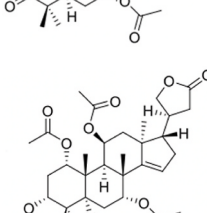
Table 2

Molecular docking scores and 2D structures of investigated Limonoids.

Limonoids	2D structure of compound	FK506 Binding Protein 35 (kcal/mol)
1		−6.3
2		−5.0
3		−0.4
4		−1.8
5		−2.6
6		−3.8
7		−4.9
8		−0.4

(continued on next page)

Table 2 (*continued*)

Limonoids	2D structure of compound	FK506 Binding Protein 35 (kcal/mol)
9		−1.5
10		−3.1
11		−5.4
12		2.4
13		−1.2
14		−3.1
15		−5.1
16		−2.5
D51		−6.1

3.2. Dynamical behavior of compounds upon ligation
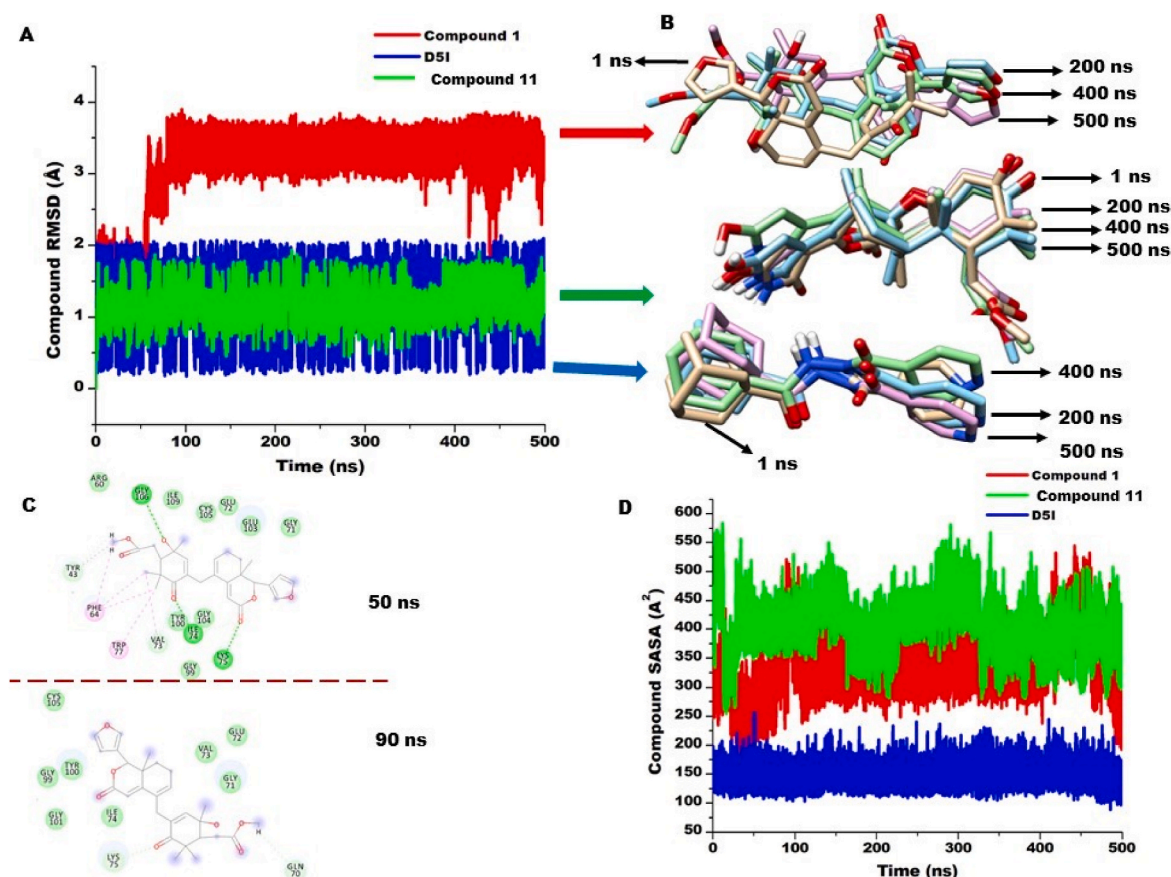
3.2.1. Compounds stability

The root mean-square deviations of the atoms which is reflective of the stability [128,129] of the compounds within the binding pocket were estimated over the 500 ns period of simulation. The deviations were computed relative to the C- α atoms starting positions which presented 1.18 ± 0.19 Å, 3.12 ± 0.60 Å and 1.31 ± 0.35 Å as average RMSD values for compound **1**, compound **11** and the D5I respectively. Fig. 1 depicts the graphical representations of the stability of the compounds over time. As observed from the Figure, Compound **11** and D5I showed uniformity in motions over the entire simulation period. Compound **1,** however, showed a variation in motions. This is can be as a result of loss of electrostatic interactions as loss of electrostatic interaction increases the dynamics of a complex [130] It exhibited similar motions with the other compounds in the first 70 ns but underwent a changed motions trajectory (70 ns to about 90 ns) and became stable afterwards. This sharp change in motions underscores the limitations of the docking method employed wherein the protein was considered fixed while the compounds were taken as conformationally flexible [131, 132]. Molecular dynamics thus addresses this shortcoming by providing the space for both compounds and proteins to assume flexibility as observed in biological systems [133]. The realignment of compound **11** to a more favourable conformation during this course could account for the observed different behavior relative to the other compounds and hence the elevated average RMSD value. Further investigating this, snapshots before, during and after the period of change were taken and visualized. The snapshots revealed compound **11** rotated 180° after 70 ns buttressing the graphical representation and the differential in RMSD values. Generally, these compounds stabilized upon binding into the pocket of FKBP.

3.2.2. Compounds' deeper penetration stabilizes PvFKBP35 Binding site

The SASA metric which could be used to evaluate the degree of penetration of the compounds into the hydrophobic core of the protein was assessed and presented in Fig. 2C. This was premised on the hypothesis that the deeper the penetration the lesser the surface area available for solvent interaction [134]. Average SASA values of 327.88 ± 47.54 A^2, 402.18 ± 39.81 A^2 and 148.33 ± 14.19 A^2 was shown for Compound **1**, compound **11** and D5I respectively. These results suggest D5I had the least surface area available for protein-compound extra molecular interactions while compound **11** had the highest. Though this metric has been used widely to assess the penetration of the compounds into binding cavities, the molecular weight and size of the compounds could also influence the SASA values as observed in this study wherein D5I and compound **11** had the least and highest molecular weight and size respectively. After obtaining the behavior of the compounds within the binding site we further probed the interactions between the compounds and the site residues that conditioned these varying conducts.

3.3. Molecular interactions underscoring the binding mechanism of identified Limonoids

Underlying the binding of compounds to their target protein are bond formations between the compounds and the hosting residues. The type of bonds formed highlight the therapeutic effects exhibited by the complexing [135,136]. As such, the nature and type of interactions these compounds engaged in was investigated. This was achieved through visual observations of snapshots at specific time frames of the simulation. These snapshots reveal events that manifest at those times of the simulations. Thus, snapshots were sampled from 100 ns, 300 ns, 400 ns and 500 ns. The results are shown in Fig. 2. It was observed that the compounds engaged in varying bond type formations ranging from strong conventional and carbon hydrogen bonds, pi sigma and alkyl to van der Waals. For compound **1**, Asp55 was observed to interact with it through conventional hydrogen bonds at 300 ns and 400 ns (Table 3).

Fig. 1. Comparative representation of the stability, motion and SASA of the compounds and D5I A) shows the RMSD plots of compound **1** (red) compound **11** (green) and D5I (blue), plots show stability of the compounds over the simulation period. B) shows snapshot of the motions of compounds over the simulation period. C) show the visual differential positions of compound 1 at 50 ns and 90 ns. Snapshots show a 180° repositioning of the compound. D) shows the graphical representation of solvent accessibility (SASA) of the compounds. (For interpretation of the references to colour in this figure legend, the reader is referred to the Web version of this article.)

Arg60 was also observed to form conventional hydrogen bond with the compounds at 400 ns while Gly104 formed carbon hydrogen bonds at 300 ns and 400 ns. Other residues such as Tyr43, Phe54, Phe64, Ile74, Trp77, Tyr100, Ile109, Pro110, Leu115 and Phe117 engaged in relatively weaker interactions involving alkyl and pi alkyl at varying times of the simulation. At 300 ns, Cys105 was observed to engage in pi-sulfur interactions with compound **1**.

Similar interactions were observed to exist between compound **11** and the site residues. Asp55 interacted through conventional hydrogen bonds at 100 ns (Table 3) whiles Tyr100 at 100 ns and 400 ns. Gly104 formed a carbon hydrogen bonds at 300 ns and conventional hydrogen bond 400 ns and 500 ns. Ser108 also observed to form conventional hydrogen bonds with the compound at 300 ns. Gly106 and Pro110 formed carbon hydrogen bonds at 300 ns and 500 ns respectively.

Juxtaposing these observations with the interactions that underlie the potency of D5I, it was observed that D5I engaged in stable hydrogen bonds with critical residues that endured through the simulation period. Glu72, Ile74 and Tyr100 formed conventional hydrogen bonds that were observed in all the assembled snapshots. Val73 also consistently formed carbon hydrogen bond with D5I as observed in the assembled snapshots. However, Gly71 formed carbon hydrogen bonds at 300 ns and 500 ns only. Tyr43, Phe64, Trp77 and Phe117 engaged in pi and alkyl interactions with D5I at varying times of the simulation. These observations are critical and would be useful in compounds optimization to achieve maximum therapeutic effects. Since snapshots represent events at a specific time of the simulation period, we sought to buttress our observation by computing the hydrogen bond occupancy (fraction of simulation), the average bond distance, and bond angle of the hydrogen

bonds. The results are presented in Table 3 This computation (high percentage occupation) corroborated the earlier observation in which Asp55, Ile74 and Tyr100 featured the most via hydrogen bonding. Having determined the behavior of the compounds within the binding site and the interactions that characterize them, we probed their impact on the conformational dynamics of the binding cavity.

3.4. Binding site dynamics upon ligation

The effects of the interactions that occurred between the compounds and site residues influence the conformations of the binding site. These change in conformations at the immediate regions of the compounds translate into signals that resultantly induce therapeutic effects [137]. The RMSD of the C-α atoms of the site residues and their SASA were then computed. These provided insights into the stability and the hydrophobicity of the binding pocket upon ligation. As observed in Fig. 3, the compounds including D5I stabilized the binding site. Average RMSD values of 1.83 ± 0.19 Å, 2.78 ± 0.48 Å, 1.68 ± 0.36 Å and 3.40 ± 0.75 Å for compound **1** complex, compound **11** complex, D5I complex and the unbound site respectively suggesting that D5I induced the highest stability of the site while the unbound was highly unstable. These differentials in stability exhibited by the compounds relative to D5I could be due to the type of interactions that underlined their complexing wherein stronger and consistent bonds were observed for D5I. The SASA of the binding site also revealed the compounds influence a reduction in the surface area of the pocket available for solvent interactions. They presented average SASA values of 1328.08 ± 109.27 Å^2, 1466.33 ± 105.80 Å^2, 1321.69 ± 80.09 Å^2 and 1505.16 ± 76.12 Å^2 for compound **1**
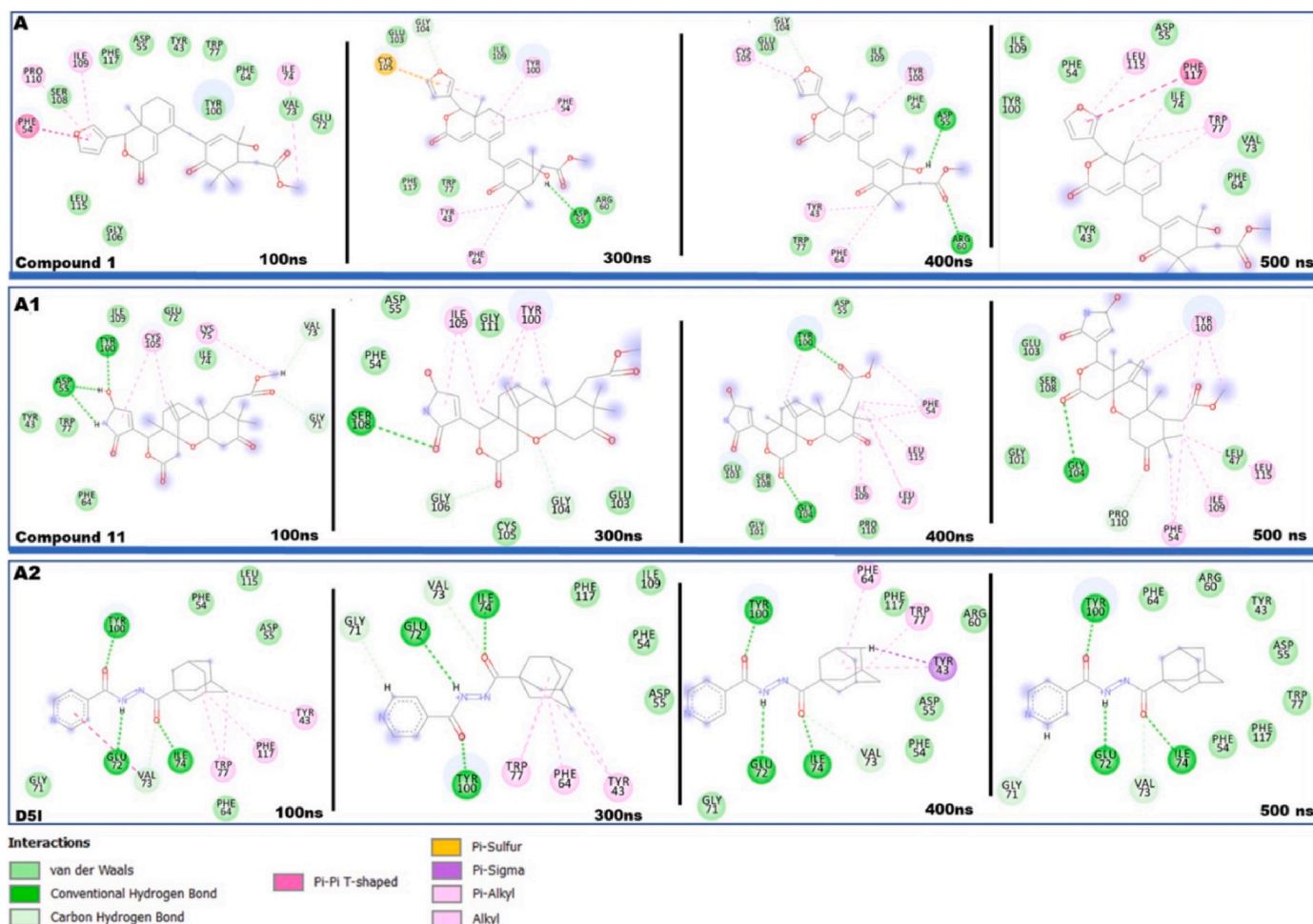
Fig. 2. 2D visualization of snapshots of the compounds over the period of simulation sampled from 100 ns, 300 ns, 400 ns and 500 ns.

Table 3
Dynamic hydrogen bond interactions of the compounds at the binding site.

| Compounds	H-Acceptor	H-Donor	Occupancy (%)	Distance (Å)	Angle (°)
Compound **1**	ASP55-OD2	LIGAND-O2	26.29	2.76	164
	ASP55-OD1	LIGAND-O2	10.60	2.7	163
Compound **11**	ASP55-0D2	LIGAND-O4	16.93	2.62	167
	PHE54-O	LIGAND-O4	10.80	2.69	161
D5I	LIGAND-O16	TYR100-OH	71.21	2.79	164
	LIGAND-O1	ILE74-N	67.24	2.86	156
	GLU72-O	LIGAND-N14	25.12	2.90	159

complex, compound **11** complex, D5I complex and the unbound site respectively. Again, the D5I complex site showed the least available surface area while the unbound showed the highest (Fig. 3). Collectively, these findings on the binding site dynamics suggest the compounds induce effects on the binding site of FKBP and serve as efficient inhibitors upon modifications.

3.5. FKBP global protein perturbations upon ligation

The global conformations of the protein were also investigated to determine the impact of the compounds binding on the global structure. This was achieved through estimating the motions and stability of the protein through the RMSD, the root mean square fluctuations (RMSF), the radius of gyration (RoG) and the SASA of the C-α atoms. Investigation of the deviations of the C-α atoms relative to the starting structure revealed the binding of the compounds including D5I induced stability of the system in reference to the unbound protein. Average RMSD values of 1.83 ± 0.34 Å, 1.49 ± 0.27 Å, 1.32 ± 0.28 Å and 2.10 ± 0.48 Å for compound **1**- FKBP complex, compound **11**- FKBP, D5I- FKBP complex and the unbound protein respectively as presented in Fig. 4A. These values fall below 2.5 Å which have been reported by several studies as the optimal threshold for a well simulated system [138–140]. These values thus repose confidence on the on the process and the conclusions derived herein. The RMSF, which is reflective of the flexibility of the protein at the individual residues revealed average values of 12.60 ± 3.83 Å, 13.14 ± 4.14 Å, 13.11 ± 3.98 Å, and 13.16 ± 3.99 Å for compound **1**- FKBP complex, compound **11**- FKBP complex, D5I- FKBP complex and the unbound protein respectively. These results suggest the binding of the compound could have a decreasing effect on the residue flexibility of the protein. Compound **1** complex showed the least values indicating the residues were least flexible followed by D5I complex and then compound **11** complexes. As observed in Fig. 4B, compound **11** exhibited the highest peaks in fluctuations at the loop regions. Differential fluctuations were also observed in other regions of the protein as presented graphically in Fig. 4B. These differentials relative to the unbound protein could underlie the compounds inhibitory potentials.

Further investigation of the radius of gyration of the C-α atoms revealed the compounds binding induced an increase in the gyrations of
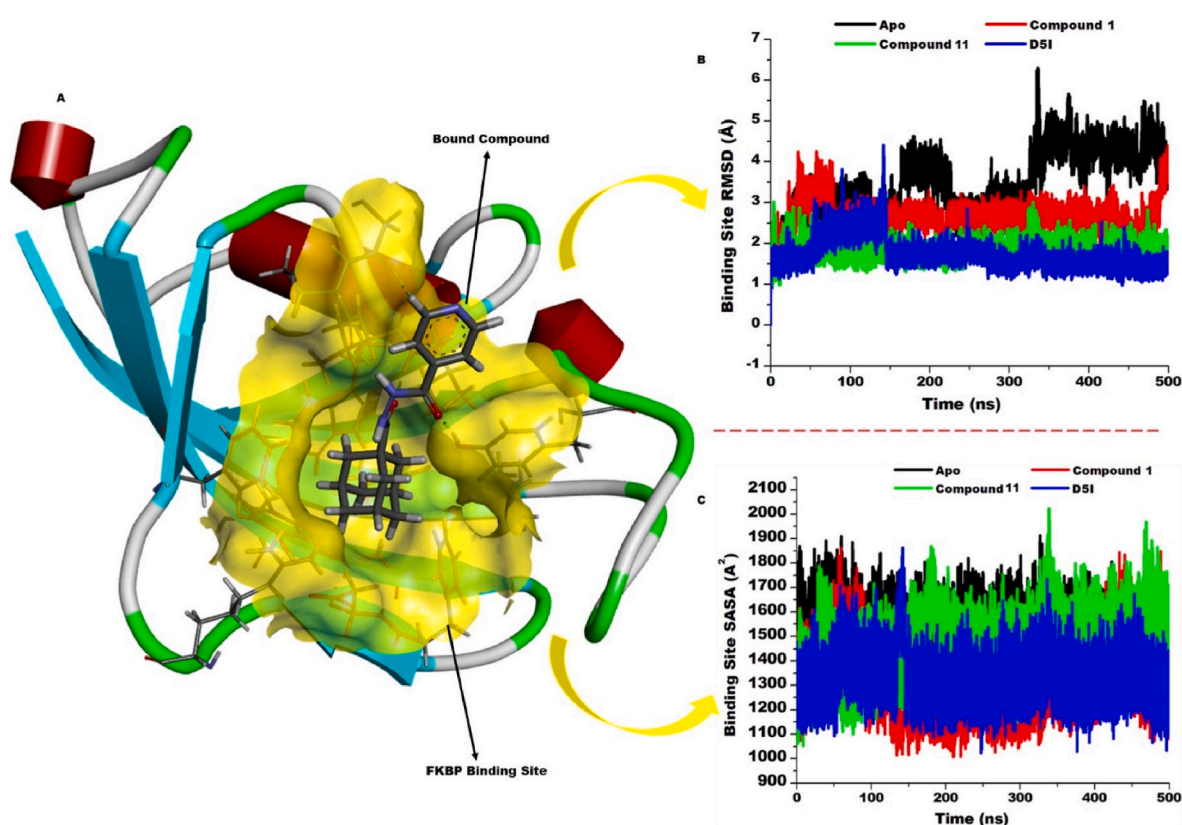
Fig. 3. Comparative analysis of the binding site dynamics of FKBP binding site upon the compounds binding. A) shows the FKBP protein highlighting the binding site of the compounds. B) shows the graphical representation of the binding site stability over the period of simulation upon bind of the compounds relative to the unbound. C) shows the graphical comparative solvent accessibility of the binding site over the period of simulation upon binding of the compounds relative to the unbound protein (Apo).

the C-α atoms. The RoG metric is informative on the compactness of the protein. The higher the radius of gyration, the lesser compact the protein [141] As observed in Fig. 4C, the complexes were less compact compared to the unbound protein. They revealed average values of 14.13 ± 0.11 Å, 14.07 ± 0.08 Å, 14.06 ± 0.08 Å and 14.32 ± 0.11 Å for Compound **1** complex, compound **11** complex, D5I complex and the unbound protein respectively. These results corroborate with the RMSF finding in which reduced fluctuations of the bound protein were observed relative to the unbound. With these findings we delved further to examine the folding or unfolding events of the protein through the SASA metric. An increase in the SASA of the protein suggests an unfolding event wherein regions of the protein hitherto unavailable for solvent interaction have become available and vice versa [134]. The investigation revealed average surface areas of 6084.26 ± 217.49, 6161.10 ± 180.83, 6089.01 ± 191.57 and 6175.57 ± 172.61 for compound **1** complex, compound **11** complex, D5I complex and the un-bound protein respectively suggesting folding of the protein occurred upon the binding of the compounds. As observed in the graphical rep-resentation in Fig. 4D and the average values, the surface available for aqueous interactions was the least in compound **1** complex and highest in the unbound protein. These findings thus reinforce the observations in the protein fluctuations and compactness. Taken together, the confor-mational dynamics presented suggest the compounds significantly per-turb the protein structure thus underscoring their therapeutic prowess.

### 3.6. Thermodynamics estimations of the identified Limonoids

The binding energy landscape of the compounds were determined through the MM-PBSA approach due to its wide usage and efficiency [142,143]. The free binding energy is important as its indicative of the spontaneity and kinetic reactions of the compounds complexing process.

The binding energy is underscored by the interaction types that occur during and after the complexing process thus stronger and favourable interactions is expected to yield low binding free energies (most nega-tive). The energy profiles of the compounds thus determined are pre-sented in Table 2. Average binding free energies of -26.66 ± 3.84 kcal/mol, -21.02 ± 3.33 kcal/mol and -27.99 ± 2.64 kcal/mol were determined for compound **1**, compound **11** and D5I (Table 4) respec-tively suggesting that the compounds presented relatively higher total free binding energies compared to D5I. This is because of loss of elec-trostatic interactions in compound **1** and **11** complexes but a more negative binding energy does not mean better inhibition [131,144] and electrostatic interactions alone does not describe the encounter of a complex but hydrophobic interactions also contribute to the formation [130]. This seems to corroborate with the type of interactions visualized in the snapshots wherein consistent conventional hydrogen interactions were observed supported by the occupancy presented in Table 2. Generally, the binding free energies for the compounds indicate their complexing was spontaneous. van der Waals and electrostatic energies contributed significantly to the total binding energies.

3.7. In silico elucidation of the pharmacokinetic properties of identified Limonoids

The physicochemical and pharmacokinetics of potent molecules are crucial determinants of the molecules' success as therapeutic agents. Thus, these potent molecules access respective therapeutic targets in concentrations that can elicit a therapeutic response. To provide insights into the pharmacokinetics of compounds **1** and **11**, we employed *in silico* techniques to assess their absorption, distribution, metabolism, excre-tion, and toxicity (ADMET). These properties also allowed for the pre-diction of the bioavailability and ability of compounds **1** and **11** to cross
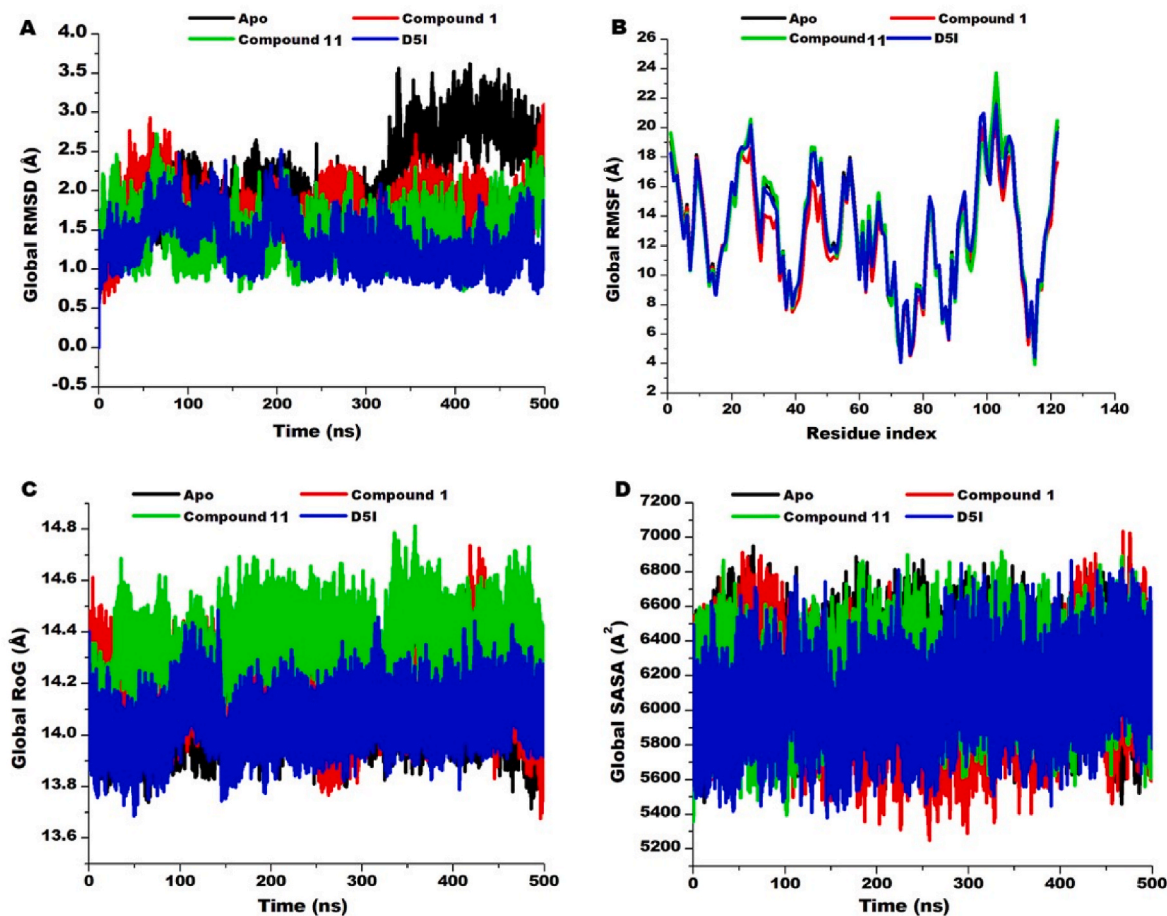
Fig. 4. Comparative analysis of the impact of the compounds on the global FKBP protein. (A) Shows the differential RMSD plots of the C-α atoms of the protein upon the compounds binding (B) Shows the residual fluctuations of the protein upon the compounds binding. (C) Shows the comparative RoG plots of the c-α atoms of the protein upon the compounds binding. (D) Shows the comparative plots of the solvent accessibility surface area (SASA) of the protein upon the compounds binding.
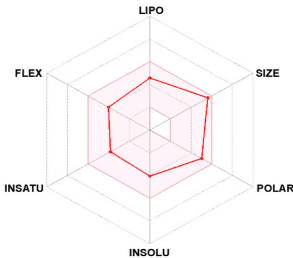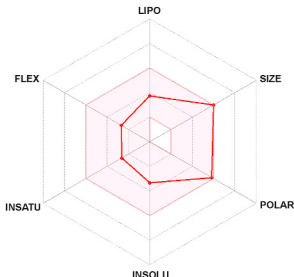
Table 4
MMPBSA calculations showing the binding energy Profile of D51, compounds **1** and **11**. ΔE_{ele} = electrostatic energy; ΔE_{vdW} = van der Waals energy; ΔG_{bind} = total binding free energy; ΔG_{sol} = solvation free energy ΔG = gas phase free energy.
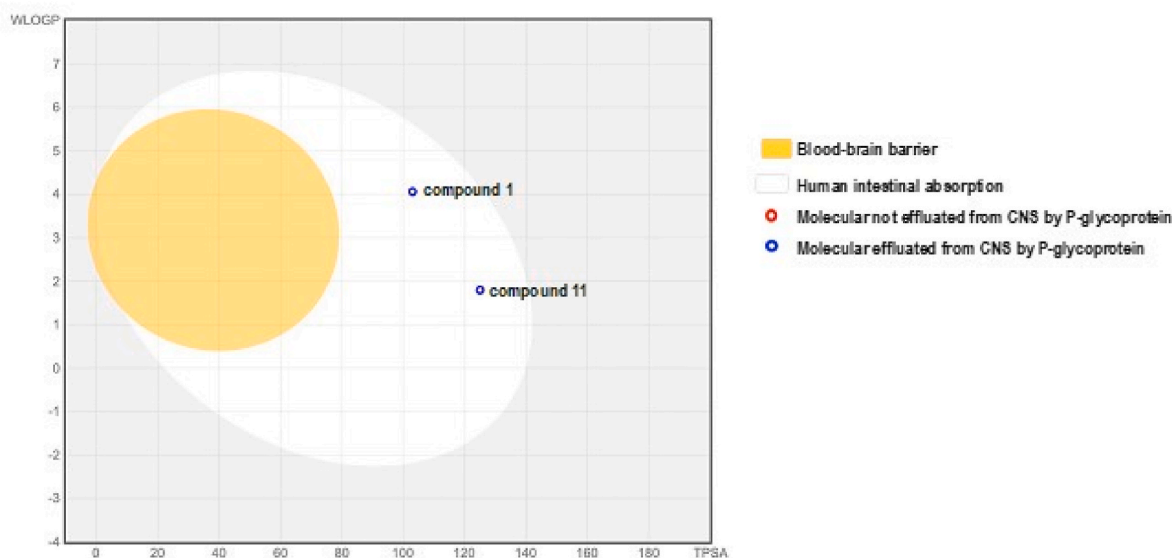
System Energy components (kcal/mol)					
	ΔE_{vdw}	ΔE_{ele}	ΔG_{gas}	ΔG_{sol}	ΔG_{bind}
Compound 1	−33.54 ± 3.19	−13.06 ± 5.77	−46.61 ± 6.28	19.95 ± 4.13	−26.66 ± 3.84
Compound 11	−28.60 ± 4.39	−6.65 ± 10.58	−35.25 ± 8.91	14.23 ± 7.66	−21.02 ± 3.33
D5I	−29.24 ± 2.43	−28.33 ± 4.25	−57.57 ± 4.50	29.58 ± 3.07	−27.99 ± 2.64

the blood-brain barrier. Over the years, computational techniques have gained prominence as valid alternatives to conventional experimental methods of predicting ADMET properties since they suffice the resource-intensive and time-consuming experimental methods [145]. Online *in silico* ADMET predictors employed in this report included SwissADME (116), AdmetSar [146], and the Protox web server [117]. Multiple platforms were employed to validate the predictions and ensure the reliability of the insights proved. Using the SwissADME, concepts and criteria followed to predict the pharmacokinetic properties of the compounds included the Lipinski's rules of five (LRO5) [147] and the Brain Or IntestinaL EstimateD permeation method (BOILED-Egg) concept [148]. The LO5 rules [molecular weight (MW) < 500 g/mol], Log P < 5, H-bond donors (HBD) < 5 and H-bond acceptors (HBA) < 10] allowed

for an initial assessment of the drug-likeness of compounds **1** and **11**, whereby a violation of more than two of the rules suggests the respective compound is not drug-likely. As shown in Table 5 both compound **1** [MW = 468.54 g/mol], Log P = 3.42, HBD = 1, and HBA = 7] and compound **11** [MW = 468.54 g/mol], Log P = 4.42, HBD = 1, and HBA = 6] and were predicted to be drug-likely evidenced by their adherence to all the LRO5. Also, based on the Brain Or IntestinaL EstimateD permeation (BOILED-Egg) concept [148] as shown in Fig. 5, both compounds were shown to fall within the chemical space that suggests their ability to cross the blood-brain barrier, possess high intestinal absorption, and a consequential high bioavailability. The favourable Log P > 5 for both compounds also correlated with favourable lipophilicity suggesting their ability to permeate lipid membranes which could intend enhance bioavailability. The favourable lipophilicity of both compounds also suggests the compounds could possess minimal toxicities since highly lipophilic compounds tend to bind to hydrophobic targets other than the desired target [149]. The MW below 500 for both compounds could contribute to high bioavailability since small molecular weighted compounds would easily permeate intestinal epithelium to access targets with minimal off-target binding [150]. The predicted topological polar surface area (TPSA) below 140 Å^2 for both compounds suggest that they could easily be transported across cell membranes since the calculation of TPSA considers the polar atoms on the surfaces of compounds whereby compounds possessing TPSA above 140 Å^2 tend to exhibit poor cell membrane permeability [151–153]. A prediction of the LD_{50} of both compounds using the ProTox platform showed LD_{50} of 555 mg/kg and 10000 mg/kg for both compound **1** and **11** respectively. This suggested that compound **1** possesses minimal oral toxicity tendencies

Table 5
Physicochemical and Pharmacokinetic profiling of compound **1** and **11** generated from SwissADME.

Properties	compound 1	compound 11
Chemical formula	C27H32O7	C27H33NO8
Molecular weight(g/mol)	468.54	468.58
Number of heavy atoms	34	36
Number aromatic heavy atoms	5	0
Number of rotatable bonds	6	4
Number of H-bond acceptors	7	8
Number of H-bond donors	1	1
TPSA(A^2)	103.04	125.07
Molar Refractivity	125.11	130.61
$\text{LogP}_{o/w}$	3.42	2.21
LD50 mg/kg	555	10000
Bioavailable Radar		

Fig. 5. "BOILED-EGG representation of the ADME properties of compound **1** and **11** with subclassified as yolk (i.e., the physicochemical space for highly probable BBB permeation) and the white (i.e., the physicochemical space for highly probable HIA absorption).

while compound **11** was predicted to present no toxicity since molecules with LD_{50} of 0–50 mg/kg is considered highly toxic [154], whereas compounds with above 2000 mg/kg present no toxicity.

The compounds were also computationally explored to assess their ability to be retained in the central nervous system (CNS). As presented in the BOILED-EGG analysis, both compounds were predicted to be substrates of P-glycoprotein and hence could be effluxed out of the CNS back into the capillary lumen via P-glycoprotein mediation. Considering the crucial role of P-glycoprotein as an ATP-binding cassette (ABC) transporter that extruding toxins and xenobiotics out of cells, it could be inferred that both compounds would not be retained in high amounts within the CNS hence reducing their favourable absorption and bioavailability in the CNS. Overall, the predicted pharmacokinetics suggested compounds **1** and **11** are drug-like compounds with high intestinal absorption ability, minimal toxicity tendencies and could not be retained in the CNS.

3.8. Biological activity prediction of lead compounds

In order to determine the antimalarial properties of compounds **1** and **11**, Prediction of Activity Spectra for Substances (PASS) was employed [118], which estimates the probable biological activity of compounds liaising Quantitative Structure - Activity Relationship (QSAR). Compounds predicted with probable of active (Pa) greater than probable of inactive (Pi) are worth exploring [118,155,156]. Both compounds **1** and **11** were predicted to be antiprotozoal with Pa and Pi values 0.207 and 0.099 and, 0.162 and 0.155 respectively. *Plasmodium* parasites are protozoans hence antiprotozoal compounds are plausible antimalarial compounds [157]. Antiparasitic compounds have been shown in a previous study to possess antimalarial properties by killing the ring stage of *Plasmodium falciparum* and also retains activity against artemisinin resistant parasites [158]. Compounds **1** and **11** are structurally similar to moxidectin, an antiparasitic compound.

4. Conclusion

In this study, the inhibitory activity of isolated limonoids from the stem barks of *Entadrophragma angolense* against *Pv*FKBD35 was explored. Sixteen [16] limonoids were docked against the energy minimized PvFKBD35. Compounds **1** and **11** showed favourable predicted binding affinities and interacted with the critical residues of *Pv*FKBD35 throughout the 500 ns MD simulation. The RMSD, RMSF, RoG and SASA provided insights into the stability and the conformational dynamics of the *Pv*FKBD35 upon binding of compound **1** and **11**. These showed that the binding of both compounds perturbed the structure of Pv FKBD35 which could underpin the binding potential of both compounds. Assessment of the pharmacokinetics of the compounds furthers highlighted their therapeutic potential by adhering to the Lipinski's rules of 5, high intestinal absorption with minimal to no toxicities. Compounds **1** and **11** were also predicted to be antiprotozoal making them plausible antimalarial compounds. Nonetheless, additional experimental validation is required to further establish the binding potential of these compounds. This findings in the interim however, could serve as preliminary data towards the development of novel *Pv*FKBD35 inhibitors as therapeutics against *P. vivax*.

Availability of data and materials

All data generated and analyzed during this study are included in this manuscript and the supplementary data.

Authors contributions

Conceptualization-LA, Computational Analysis & Methodology-ARI & CA with contribution from MA, Writing-original draft-LA, CA & ARI, Supervision-DOY, SM & MMB, Funding acquisition-MMB, Writing-review and editing- LA, KAK, MA, DOY, & MMB.

Declaration of competing interest

The authors declare that they have no known competing financial interests or personal relationships that could have appeared to influence the work reported in this paper.

References

[1] Word WHO. Malaria report 2021. Word malaria report. Geneva: World Health Organization; 2021. Licence: CC. 2021. 2013–2015.

[2] Malaria [Internet]. [cited 2020 Jul 2]. Available from: https://www.who.int/health-topics/malaria/?tab=tab_1.

[3] Recker M, Bull PC, Buckee CO [Internet]. Recent advances in the molecular epidemiology of clinical malaria, vol. 7. F1000Research. F1000 Research Ltd; 2018 [cited 2020 Jul 3]. Available from:/pmc/articles/PMC6073089/?report=abstract.

[4] Fikadu M, Ashenafi E. Malaria: an overview. Infect drug resist [Internet]. 2023 [cited 2023 Jul 22];16:3339. Available from:/pmc/articles/PMC10237628/.

[5] Escalante AA, Cepeda AS, Pacheco MA. Why Plasmodium vivax and Plasmodium falciparum are so different? A tale of two clades and their species diversities. Malar J 2022;211 [Internet]. 2022 May 3 [cited 2023 Jul 21];21(1):1–19. Available from: https://malariajournal.biomedcentral.com/articles/10.1186/s12936-022-04130-9.

[6] Andrews KT, Fisher G, Skinner-Adams TS. Drug repurposing and human parasitic protozoan diseases. In: International journal for parasitology: drugs and drug resistance. vol. 4. Elsevier Ltd; 2014. p. 95–111.

[7] Weiss DJ, Lucas TCD, Nguyen M, Nandi AK, Bisanzio D, Battle KE, et al. Mapping the global prevalence, incidence, and mortality of Plasmodium falciparum, 2000–17: a spatial and temporal modelling study. Lancet 2019 Jul 27;394 (10195):322–31.

[8] Tizifa TA, Kabaghe AN, McCann RS, van den Berg H, Van Vugt M, Phiri KS. Prevention Efforts for Malaria [Internet] Current tropical medicine reports. Springer Verlag 2018;vol. 5 [cited 2020 Jul 7]. pp. 41–50. Available from:/pmc/articles/PMC5879044/?report=abstract.

[9] Hawadak J, Dongang Nana RR, Singh V. Global trend of Plasmodium malariae and Plasmodium ovale spp. malaria infections in the last two decades (2000–2020): a systematic review and meta-analysis [Internet] Parasit Vectors 2021 Dec 1 [cited 2023 Jul 22];14(1):297. Available from:/pmc/articles/PMC8173816/.

[10] White NJ. Plasmodium knowlesi: the fifth human malaria parasite [Internet] Clin Infect Dis 2008 Jan 15 [cited 2020 Jul 7];46(2):172–3. Available from: https://academic.oup.com/cid/article-lookup/doi/10.1086/524889.

[11] Jongwutiwes S, Buppan P, Kosuvin R, Seethamchai S, Pattanawong U, Sirichaisinthop J, et al. Plasmodium knowlesi malaria in humans and macaques, Thailand. Emerg Infect Dis [Internet; 2011. https://doi.org/10.3201/eid1710.110349 [cited 2020 Jul 7];17(10):1799–806.

[12] Singh B, Daneshvar C. Human infections and detection of plasmodium knowlesi [Internet]. In: Clinical microbiology reviews. vol. 26. American Society for Microbiology Journals; 2013 [cited 2020 Jul 7]. pp. 165–84. Available from:.

[13] Malaria [Internet]. [cited 2023 Jul 31]. Available from: https://www.who.int/health-topics/malaria/#tab=tab_2.

[14] Ashley EA, Pyae Phyo A, Woodrow CJ. Malaria [Internet] Lancet 2018 Apr 21 [cited 2022 Mar 13];391(10130):1608–21. Available from: http://www.thelancet.com/article/S0140673618303246/fulltext.

[15] Milner Jr DA. Malaria pathogenesis [Internet] Cold Spring Harb Perspect Med 2018 Jan 1 [cited 2022 Mar 13];8(1). Available from:/pmc/articles/PMC5749143/.

[16] Plewes K, Leopold SJ, Kingston HWF, Dondorp AM. Malaria: what's new in the management of malaria? Infect Dis Clin 2019 Mar 1;33(1):39–60.

[17] Nsanzabana C. Resistance to artemisinin combination therapies (ACTs): do not forget the partner drug [Internet] Trav Med Infect Dis 2019 Feb 1 [cited 2022 Mar 14];4(1). Available from:/pmc/articles/PMC6473515/.

[18] Coronado LM, Nadovich CT, Spadafora C. Malarial hemozoin: from target to tool [Internet] Biochim Biophys Acta 2014 [cited 2022 Mar 14];1840(6):2032–41. Available from: https://pubmed.ncbi.nlm.nih.gov/24556123/.

[19] Bridgford JL, Xie SC, Cobbold SA, Pasaje CFA, Herrmann S, Yang T, et al. Artemisinin kills malaria parasites by damaging proteins and inhibiting the proteasome. Nat Commun 2018 91 [Internet]. 2018 Sep 18 [cited 2022 Mar 14];9 (1):1–9. Available from: https://www.nature.com/articles/s41467-018-06221-1.

[20] Cui L, Su XZ. Discovery, mechanisms of action and combination therapy of artemisinin [Internet] Expert Rev Anti Infect Ther 2009 Oct [cited 2022 Mar 14]; 7(8):999. Available from:/pmc/articles/PMC2778258/.

[21] Ariey F, Witkowski B, Amaratunga C, Beghain J, Langlois AC, Khim N, et al. A molecular marker of artemisinin-resistant Plasmodium falciparum malaria. Nature 2014;505(7481):50–5.

[22] Dondorp AM, Ringwald P. Artemisinin resistance is a clear and present danger [Internet]. In: Trends in parasitology. vol. 29; 2013 [cited 2020 Apr 7]. pp. 359–60. Available from:.

[23] Dhorda M, Amaratunga C, Dondorp AM. Artemisinin and multidrug-resistant Plasmodium falciparum - a threat for malaria control and elimination [Internet] Curr Opin Infect Dis 2021 Oct 1 [cited 2022 Mar 14];34(5):432–9. Available from: https://journals.lww.com/co-infectiousdiseases/Fulltext/2021/10000/Artemisinin_and_multidrug_resistant_Plasmodium.8.aspx.

[24] Kozlov M. Resistance to front-line malaria drugs confirmed in Africa. Nature 2021 Sep 1;597(7878):604.

[25] Nsanzabana C. Time to scale up molecular surveillance for anti-malarial drug resistance in sub-saharan Africa [Internet] Malar J 2021 Dec 1 [cited 2022 Mar 30];20(1):1–5. Available from: https://malariajournal.biomedcentral.com/articles/10.1186/s12936-021-03942-5.

[26] Siddiqui FA, Liang X, Cui L. Plasmodium falciparum resistance to ACTs: emergence, mechanisms, and outlook. Int J Parasitol Drugs Drug Resist 2021 Aug 1;16:102–18.

[27] Yasri S, Wiwanitkit V. Artemisinin resistance: an important emerging clinical problem in tropical medicine [Internet] Int J Physiol Pathophysiol Pharmacol 2021 [cited 2022 Mar 30];13(6):152. Available from:/pmc/articles/PMC8784654/.

[28] Okpeku M. Adaptive drug resistance in malaria parasite: a threat to malaria elimination agenda? Plasmodium species drug resist [Internet]. 2021. Jun 4 [cited 2022 Mar 30]; Available from: https://www.intechopen.com/chapters/77047.

[29] Uzor PF, Prasasty VD, Agubata CO. Natural products as sources of antimalarial drugs. Evid base Compl Alternative Med 2020;2020.

[30] Tajuddeen N, Van Heerden FR. Antiplasmodial natural products: an update. Malar J 2019;181 [Internet]. 2019 Dec 5 [cited 2022 Mar 30];18(1):1–62. Available from: https://malariajournal.biomedcentral.com/articles/10.1186/s12936-019-3026-1.

[31] Wells TNC. Natural products as starting points for future anti-malarial therapies: going back to our roots? Malar J 2011 Mar;10(SUPPL. 1):1–12.

[32] Newman DJ, Cragg GM. Natural products as sources of new drugs over the 30 years from 1981 to 2010. J Nat Prod 2012;75:311–35.

[33] Kayser O, Kiderlen AF, Croft SL [Internet]. Natural products as antiparasitic drugs, vol. 90. Parasitology Research; 2003 [cited 2020 Apr 8]. p. S55-62. Available from: http://www.ncbi.nlm.nih.gov/pubmed/12937967.

[34] Potterat O, Hamburger M. Drug discovery and development with plant-derived compounds. Prog Drug Res 2008;65:46–118.

[35] Dias DA, Urban S, Roessner U [Internet]. A Historical overview of natural products in drug discovery, vol. 2. Metabolites. MDPI AG; 2012 [cited 2021 Apr 6]. pp. 303–36. Available from:/pmc/articles/PMC3901206/.

[36] Boadu AA, Asase A. Documentation of herbal medicines used for the treatment and management of human diseases by some communities in Southern Ghana [Internet] Evid Based Complement Alternat Med 2017 [cited 2020 Apr 13];2017: 3043061. Available from: http://www.ncbi.nlm.nih.gov/pubmed/28684965.

[37] Calixto JB. Twenty-five years of research on medicinal plants in Latin America: a personal view [Internet]. Journal of ethnopharmacology, vol. 100. Elsevier Ireland Ltd; 2005 [cited 2020 Apr 13]. pp. 131–4. Available from: http://www.ncbi.nlm.nih.gov/pubmed/16006081.

[38] Mohammadi S, Jafari B, Asgharian P, Martorell M, Sharifi-Rad J. Medicinal plants used in the treatment of Malaria: a key emphasis to Artemisia, Cinchona, Cryptolepis, and Tabebuia genera [Internet] Phyther Res 2020 Jul 1 [cited 2022 Mar 18];34(7):1556–69. Available from: https://onlinelibrary.wiley.com/doi/full/10.1002/ptr.6628.

[39] Mintah SO, Archer M-A, Asafo-Agyei T, Ayertey F, Jnr PA-A, Boamah D, et al. Medicinal plant use in Ghana: advancement and challenges [Internet] Am J Plant Sci 2022. Mar 9 [cited 2023 Jul 31];13(3):316–58. Available from: http://www.scirp.org/journal/PaperInformation.aspx?PaperID=115859.

[40] Mouthé Happi G, Tchaleu Ngadjui B, Green IR, Fogué Kouam S. Phytochemistry and pharmacology of the genus Entandrophragma over the 50 years from 1967 to 2018: a 'golden' overview [Internet] J Pharm Pharmacol 2018 Nov 1 [cited 2022 Mar 18];70(11):1431–60. Available from: https://onlinelibrary.wiley.com/doi/full/10.1111/jphp.13005.

[41] Ugboduma AO, Adu F, Agyare C, Annan K, Osei-Asante S. Phytochemical screening and antimicrobial activity of Entandrophragma angolense [Internet] J Pharm Nutr Sci 2013 Aug 5 [cited 2022 Mar 18];3(4):241–9. Available from: https://setpublisher.com/pms/index.php/jpans/article/view/1586.

[42] Koul O, Daniewski WM, Multani JS, Gumulka M, Singh G. Antifeedant effects of the limonoids from Entandrophragma candolei (Meliaceae) on the gram pod borer, Helicoverpa armigera (Lepidoptera: noctuidae) [Internet] J Agric Food Chem 2003 Dec 3 [cited 2022 Mar 18];51(25):7271–5. Available from: https://pubmed.ncbi.nlm.nih.gov/14640569/.

[43] Njar VCO, Adesanwo JK, Raji Y. Methyl angolensate: the antiulcer agent of the stem bark of Entandrophragma angolense [Internet] Planta Med 1995 Jan 4 [cited 2022 Mar 18];61(1):91–2. Available from: http://www.thieme-connect.de/DOI/DOI?10.1055/s-2006-958015.

[44] Oyawaluja BO, Oyawaluja AA, Babasanmi Bc JS, Soneye OB. Phytochemistry and antioxidant assays of Entandrophragma angolense (Welw.) C.DC. (meliaceae) using DPPH and nitric oxide free radical scavenging methods [Internet] Niger J Pharm Res 2020 Jan 30 [cited 2022 Mar 18];15(2):229–35. Available from: https://www.ajol.info/index.php/njpr/article/view/192664.

[45] Chen LC, Liao HR, Chen PY, Kuo WL, Chang TH, Sung PJ, et al. Limonoids from the seeds of swietenia macrophylla and their anti-inflammatory activities. Mol 2015;20:18551–64 [Internet]. 2015 Oct 12 [cited 2022 Mar 18];20(10): 18551–64. Available from: https://www.mdpi.com/1420-3049/20/10/18551/htm.

[46] Chen JJ, Huang SS, Liao CH, Wei DC, Sung PJ, Wang TC, et al. A new phragmalin-type limonoid and anti-inflammatory constituents from the fruits of Swietenia macrophylla. Food Chem 2010 May 15;120(2):379–84.

[47] Bickii J, Tchouya GRF, Tchouankeu JC, Tsamo E. The antiplasmodial agents of the stem bark of Entandrophragma angolense (meliaceae) [Internet] African J Tradit complement alternant med 2007 [cited 2022 Mar 18];4(2):135. Available from:/pmc/articles/PMC2816453/.

[48] Mukaila YO, Oladipo OT, Ogunlowo I, Ajao AAN, Sabiu S. Which plants for what ailments: a quantitative analysis of medicinal ethnobotany of Ile-Ife, Osun State, Southwestern Nigeria [Internet] Evid Based Complement Alternat Med 2021 [cited 2022 Mar 31];2021. Available from:/pmc/articles/PMC8355999/.

[49] Kamkumo RG, Betene ANM, Fokou PVT, Donfack JH, Nangap MJT, Ngako A, et al. Antimalarial effects of the aqueous extract of Entandrophragma angolense bark on plasmodium berghei infection in mice. Pharmacogn J 2020 Jun 1;12(4): 687–98.

[50] Fan W, Fan L, Wang Z, Yang L. Limonoids from the genus melia (Meliaceae): phytochemistry, synthesis, bioactivities, pharmacokinetics, and toxicology. Front Pharmacol 2022 Jan 24;12:3785.

[51] Amoa Onguéné P, Ntie-Kang F, Lifongo LL, Ndom JC, Sippl W, Mbaze LMA. The potential of anti-malarial compounds derived from African medicinal plants, part I: a pharmacological evaluation of alkaloids and terpenoids [Internet] Malar J 2013 Dec 13 [cited 2022 Mar 19];12(1):1–26. Available from: https://malariajournal.biomedcentral.com/articles/10.1186/1475-2875-12-449.

[52] Zhang WY, An FL, Zhou MM, Chen MH, Jian KL, Quasie O, et al. Limonoids with diverse frameworks from the stem bark of Entandrophragma angolense and their bioactivities [Internet] RSC Adv 2016 Oct 10 [cited 2022 Mar 19];6(99): 97160–71. Available from: https://pubs.rsc.org/en/content/articlehtml/2016/ra/c6ra19532f.

[53] Barth S, Nesper J, Hasgall PA, Wirthner R, Nytko KJ, Edlich F, et al. The peptidyl prolyl cis/trans isomerase FKBP38 determines hypoxia-inducible transcription factor prolyl-4-hydroxylase PHD2 protein stability. Mol Cell Biol 2007 May;27 (10):3758–68.

[54] Choi B-H, Feng L, Yoon HS. FKBP38 protects Bcl-2 from caspase-dependent degradation. J Biol Chem 2010 Mar;285(13):9770–9.

[55] Jinwal UK, Koren 3rd J, Borysov SI, Schmid AB, Abisambra JF, Blair LJ, et al. The Hsp90 cochaperone, FKBP51, increases Tau stability and polymerizes microtubules. J Neurosci Off J Soc Neurosci 2010 Jan;30(2):591–9.

[56] Banasavadi-Siddegowda YK, Mai J, Fan Y, Bhattacharya S, Giovannucci DR, Sanchez ER, et al. FKBP38 peptidylprolyl isomerase promotes the folding of cystic fibrosis transmembrane conductance regulator in the endoplasmic reticulum. J Biol Chem 2011 Dec;286(50):43071–80.

[57] Ahearn IM, Tsai FD, Court H, Zhou M, Jennings BC, Ahmed M, et al. FKBP12 binds to acylated H-ras and promotes depalmitoylation. Mol Cell 2011 Jan;41(2): 173–85.

[58] Shirane M, Nakayama KI. Inherent calcineurin inhibitor FKBP38 targets Bcl-2 to mitochondria and inhibits apoptosis. Nat Cell Biol 2003 Jan;5(1):28–37.

[59] Cameron AM, Steiner JP, Sabatini DM, Kaplin AI, Walensky LD, Snyder SH. Immunophilin FK506 binding protein associated with inositol 1,4,5-trisphosphate receptor modulates calcium flux. Proc Natl Acad Sci U S A 1995 Feb;92(5): 1784–8.

[60] Riggs DL, Roberts PJ, Chirillo SC, Cheung-Flynn J, Prapapanich V, Ratajczak T, et al. The Hsp90-binding peptidylprolyl isomerase FKBP52 potentiates glucocorticoid signaling in vivo. EMBO J 2003 Mar;22(5):1158–67.

[61] Wang T, Li BY, Danielson PD, Shah PC, Rockwell S, Lechleider RJ, et al. The immunophilin FKBP12 functions as a common inhibitor of the TGF beta family type I receptors. Cell 1996 Aug;86(3):435–44.

[62] Jayaraman T, Brillantes AM, Timerman AP, Fleischer S, Erdjument-Bromage H, Tempst P, et al. FK506 binding protein associated with the calcium release channel (ryanodine receptor). J Biol Chem 1992 May;267(14):9474–7.

[63] Ochocka AM, Kampanis P, Nicol S, Allende-Vega N, Cox M, Marcar L, et al. FKBP25, a novel regulator of the p53 pathway, induces the degradation of MDM2 and activation of p53 [Internet] FEBS Lett 2009 Feb 18 [cited 2023 Jul 31];583 (4):621–6. Available from: https://pubmed.ncbi.nlm.nih.gov/19166840/.

[64] Crackower MA, Kolas NK, Noguchi J, Sarao R, Kikuchi K, Kaneko H, et al. Essential role of Fkbp6 in male fertility and homologous chromosome pairing in meiosis. Science 2003 May;300(5623):1291–5.

[65] Kuzuhara T, Horikoshi M. A nuclear FK506-binding protein is a histone chaperone regulating rDNA silencing. Nat Struct Mol Biol 2004;11(3):275–83.

[66] Nelson CJ, Santos-Rosa H, Kouzarides T. Proline isomerization of histone H3 regulates lysine methylation and gene expression. Cell 2006 Sep;126(5):905–16.

[67] Rajan S, Yoon HS. Structural insights into plasmodium PPIases. Front Cell Infect Microbiol 2022 Sep 2;12:1309.

[68] Dutta T, Singh H, Edkins AL, Blatch GL. Hsp90 and associated Co-chaperones of the malaria parasite. Biomol 2022;12:1018 [Internet]. 2022 Jul 22 [cited 2023 Apr 6];12(8):1018. Available from: https://www.mdpi.com/2218-273X/12/8/1018/htm.

[69] Thommen BT, Dziekan JM, Achcar F, Tjia S, Passecker A, Buczak K, et al. FKBP35 secures ribosome homeostasis in Plasmodium falciparum. bioRxiv [Internet] 2023. Feb 17 [cited 2023 Apr 6];2022.12.09.519720. Available from: https://www.biorxiv.org/content/10.1101/2022.12.09.519720v2.

[70] Harikishore A, Niang M, Rajan S, Preiser PR, Yoon HS. Small molecule Plasmodium FKBP35 inhibitor as a potential antimalaria agent. Sci Rep 2013;31 [Internet]. 2013 Aug 26 [cited 2023 Apr 6];3(1):1–8. Available from: https://www.nature.com/articles/srep02501.

[71] Atack TC, Raymond DD, Blomquist CA, Pasaje CF, McCarren PR, Moroco J, et al. Targeted covalent inhibition of plasmodium FK506 binding protein 35. ACS Med Chem Lett 2020;11(11):2131–8.

[72] Bharatham N W, Chang M, Yoon H S. Targeting FK506 binding proteins to fight malarial and bacterial infections: current advances and future perspectives. Curr Med Chem.[Internet] 2011 Apr 25 [cited 2023 Apr 6];18(12):1874–89. Available from: https://pubmed.ncbi.nlm.nih.gov/21466465/.

[73] Kotaka M, Ye H, Alag R, Hu G, Bozdech Z, Preiser PR, et al. Crystal structure of the FK506 binding domain of Plasmodium falciparum FKBP35 in complex with FK506 [Internet] Biochemistry 2008 Jun 3 [cited 2023 Apr 6];47(22):5951–61. Available from: https://pubmed.ncbi.nlm.nih.gov/18465874/.

[74] Harikishore A, Leow ML, Niang M, Rajan S, Pasunooti KK, Preiser PR, et al. Adamantyl derivative as a potent inhibitor of Plasmodium FK506 binding protein 35 [Internet] ACS Med Chem Lett 2013 Nov 14 [cited 2023 Jul 31];4(11): 1097–101. Available from: https://pubmed.ncbi.nlm.nih.gov/24900611/.

[75] Shaker B, Ahmad S, Lee J, Jung C, Na D. In silico methods and tools for drug discovery [Internet] Comput Biol Med 2021. Oct 1 [cited 2023 Apr 5];137. Available from: https://pubmed.ncbi.nlm.nih.gov/34520990/.

[76] Jabalia N, Kumar A, Kumar V, Rani R. In Silico Approach in Drug Design and Drug Discovery: an Update. Innov Implementations Comput Aided Drug Discov Strateg Ration Drug Des [Internet]. 2021 [cited 2023 Apr 5];245–71. Available from: https://link.springer.com/chapter/10.1007/978-981-15-8936-2_10.

[77] Sliwoski G, Kothiwale S, Meiler J, Lowe EW. Computational methods in drug discovery [Internet] Pharmacol Rev 2014 Jan [cited 2023 Mar 27];66(1):334. Available from:/pmc/articles/PMC3880464/.

[78] Adams L, Afiadenyo M, Kwofie SK, Wilson MD, Kusi KA, Obiri-Yeboah D, et al. In silico screening of phytochemicals from Dissotis rotundifolia against Plasmodium falciparum Dihydrofolate Reductase. Phytomedicine Plus [Internet]. 2023 May 1 [cited 2023 Apr 6];3(2):100447. Available from: https://linkinghub.elsevier.com/retrieve/pii/S266703132300043X.

[79] Pereira CA, Sayé M, Reigada C, Silber AM, Labadie GR, Miranda MR, et al. Computational approaches for drug discovery against trypanosomatid-caused diseases [Internet] Parasitology 2020 May 1 [cited 2023 Mar 27];147(6):611–33. Available from: https://www.cambridge.org/core/journals/parasitology/article/abs/computational-approaches-for-drug-discovery-against-trypanosomatid-caused-diseases/18737812181210374FED1C3060C5CBA7.

[80] López-López E, Barrientos-Salcedo C, Prieto-Martínez FD, Medina-Franco JL. In silico tools to study molecular targets of neglected diseases: inhibition of TcSir2rp3, an epigenetic enzyme of Trypanosoma cruzi. 2020. p. 203–29.

[81] Berman HM, Battistuz T, Bhat TN, Bluhm WF, Philip E, Burkhardt K, et al. The protein Data Bank. Biol Crystallogr 2002;58:899–907.

[82] Pettersen EF, Goddard TD, Huang CC, Couch GS, Greenblatt DM, Meng EC, et al. UCSF chimera—a visualization system for exploratory research and analysis. J Comput Chem 2004;25:1605–12.

[83] Dwarka D, Agoni C, Mellem JJ, Soliman ME, Baijnath H. Identification of potential SARS-CoV-2 inhibitors from South African medicinal plant extracts using molecular modelling approaches. South Afr J Bot 2020 Sep 1;133:273–84.

[84] Zhang WY, An FL, Zhou MM, Chen MH, Jian KL, Quasie O, et al. Limonoids with diverse frameworks from the stem bark of Entandrophragma angolense and their bioactivities [Internet] RSC Adv 2016 Oct 10 [cited 2023 Feb 4];6(99):97160–71. Available from: https://pubs.rsc.org/en/content/articlehtml/2016/ra/c6ra 19532f.

[85] MarvinSketch. No title.. 2014.

[86] Hanwell MD, Curtis DE, Lonie DC, Vandermeerschd T, Zurek E, Hutchison GR. Avogadro: an advanced semantic chemical editor, visualization, and analysis platform. J Cheminf 2012;4(8):1–17.

[87] Trott O, Olson AJ. AutoDock Vina: improving the speed and accuracy of docking with a new scoring function, efficient optimization, and multithreading. J Comput Chem 2009;31(2) [NA-NA].

[88] Barreto Gomes DE, Galentino K, Sisquellas M, Monari L, Bouysset C, Cecchini M. ChemFlow-from 2D chemical libraries to protein-ligand binding free energies [Internet] J Chem Inf Model 2023 Jan 23 [cited 2023 Jul 23];63(2):407–11. Available from: https://pubs.acs.org/doi/full/10.1021/acs.jcim.2c00919.

[89] He X, Man VH, Yang W, Lee TS, Wang J. A fast and high-quality charge model for the next generation general AMBER force field [Internet] J Chem Phys 2020 Sep 9 [cited 2023 Jul 23];153(11):114502. Available from:/pmc/articles/PMC7728379/.

[90] Rudrapal M, Issahaku AR, Agoni C, Bendale AR, Nagar A, Soliman MES, et al. Silico screening of phytopolyphenolics for the identification of bioactive compounds as novel protease inhibitors effective against SARS-CoV-2. J Biomol Struct Dyn 2022 Nov;40(20):10437–53.

[91] Rudrapal M, Issahaku AR, Agoni C, Bendale AR, Nagar A, Soliman MES, et al. In silico screening of phytopolyphenolics for the identification of bioactive compounds as novel protease inhibitors effective against SARS-CoV-2 [Internet]. 2021 [cited 2023 May 5];40(20):10437–53. Available from: https://www.tandfo nline.com/doi/abs/10.1080/07391102.2021.1944909.

[92] Olotu FA, Agoni C, Adeniji E, Soliman M. Probing gallate-mediated selectivity and high-affinity binding of epigallocatechin gallate: a way-forward in the design of selective inhibitors for anti-apoptotic bcl-2 proteins inhibitors of lyn protein view project vesicular drug delivery systems view p. Artic Appl Biochem Biotechnol 2018 Mar;187(3):1061–80.

[93] Salmaso V, Moro S. Bridging molecular docking to molecular dynamics in exploring ligand-protein recognition process: an overview. Front Pharmacol 2018;9(August):1–16.

[94] Issahaku AR, Salifu EY, Agoni C, Alahmdi MI, Abo-Dya NE, Soliman MES, et al. Discovery of potential KRAS-SOS1 inhibitors from South African natural compounds: an in silico approach [Internet] ChemistrySelect 2023 Jun 26 [cited 2023 Jul 22];8(24):e202300277. Available from: https://onlinelibrary.wiley.co m/doi/full/10.1002/slct.202300277.

[95] Agoni C, Olotu FA, Ramharack P, Soliman ME. Druggability and drug-likeness concepts in drug design: are biomodelling and predictive tools having their say? [Internet] J Mol Model 2020 Jun 1 [cited 2023 Jul 22];26(6):1–11. Available from: https://link.springer.com/article/10.1007/s00894-020-04385-6.

[96] Case DA, Ben-Shalom IY, Brozell SR, Cerutti DS, Cheatham III TE, Cruzeiro VWD, et al. In: Amber 2018. vol. 2018. San Francisco: University of California; 2018. p. 1.

[97] Ponder JW, Case DA. Force fields for protein simulations. Elsevier; 2003.

[98] Wang J, Wolf RM, Caldwell JW, Kollman PA, Case DA. Development and testing of a general amber force field. J Comput Chem 2004 Jul;25(9):1157–74.

[99] Berendsen HJC, Postma JPM, van Gunsteren WF, DiNola a, Haak JR. Molecular dynamics with coupling to an external bath. J Chem Phys 1984;81(1984):3684–90.

[100] Hess B, Bekker H, Berendsen HJC, Fraaije JGEM. LINCS: a linear constraint solver for molecular simulations. J Comput Chem 1997;18(12):1463–72.

[101] Roe DR, Cheatham III TE. PTRAJ and CPPTRAJ: software for processing and analysis of molecular synamics trajectory data. J Chem Theor Comput 2013;9(7):3084–95.

[102] Deschenes LA. Origin 6.0: scientific Data Analysis and Graphing Software Origin Lab Corporation (formerly Microcal Software, Inc.). Web site: www.originlab. com. Commercial price: $595. Academic price: $446 J Am Chem Soc 2000 Oct;122(39):9567–8.

[103] Seifert E. OriginPro 9.1: Scientific Data Analysis and Graphing Software—Software Review [Internet] J Chem Inf Model 2014 Apr 28 [cited 2023 Jul 30];54(5):1552. Available from: https://pubs.acs.org/doi/abs/10.1021/ci500161d.

[104] Wang C, Greene D, Xiao L, Qi R, Luo R. Recent Developments and Applications of the MMPBSA Method. Front Mol Biosci 2018;4.

[105] Kuhn B, Gerber P, Schulz-Gasch T, Stahl M. Validation and use of the MM-PBSA approach for drug discovery. J Med Chem 2005 Jun;48(12):4040–8.

[106] Munsamy G, Agoni C, Soliman M. A dual target of Plasmepsin IX and X: Unveiling the atomistic superiority of a core chemical scaffold in malaria therapy:

[107] MUNSAMY et al. Lipid bilayer simulation View project. Artic J Cell Biochem 2018 May;120(5):7876–87.

[107] Agoni C, Ramharack P, Soliman MES. Co-inhibition as a strategic therapeutic approach to overcome rifampin resistance in tuberculosis therapy: Atomistic insights. Future Med Chem 2018;10(14):1665–75.

[108] Agoni C, Ramharack P, Soliman MES. Synergistic Interplay of The Co-administration of Rifampin And Newly Developed Anti-TB Drug : Could It Be a Promising New Line of TB Therapy. Comb Chem High Throughput Screen 2018;21(6):453–60.

[109] Agoni C, Ramharack P, Advances MS-R. U. Allosteric inhibition induces an open WPD-loop: a new avenue towards glioblastoma therapy. pubs.rsc.org. 2018.

[110] Olotu FA, Agoni C, Adeniji E, Abdullahi M, Soliman ME. Probing Gallate-Mediated Selectivity and High-Affinity Binding of Epigallocatechin Gallate: a Way-Forward in the Design of Selective Inhibitors for Anti-apoptotic Bcl-2 Proteins [Internet] Appl Biochem Biotechnol 2019. Mar 15 [cited 2023 Jul 23];187(3):1061–80. Available from: https://pubmed.ncbi.nlm.nih.gov/30155742/.

[111] Munsamy G, Agoni C, Soliman MES. A dual target of Plasmepsin IX and X: Unveiling the atomistic superiority of a core chemical scaffold in malaria therapy [Internet] J Cell Biochem 2019 May 1 [cited 2023 Jul 23];120(5):7876–87. Available from: https://pubmed.ncbi.nlm.nih.gov/30430636/.

[112] Agoni C, Ramharack P, Soliman MES. Co-inhibition as a strategic therapeutic approach to overcome rifampin resistance in tuberculosis therapy: atomistic insights [Internet] Future Med Chem 2018 [cited 2023 Jul 23];10(14):1665–75. Available from: https://pubmed.ncbi.nlm.nih.gov/29957065/.

[113] Agoni C, Ramharack P, Soliman MES. Synergistic Interplay of The Co-administration of Rifampin And Newly Developed Anti-TB Drug: Could It Be a Promising New Line of TB Therapy? [Internet] Comb Chem High Throughput Screen 2018 Jul 30 [cited 2023 Jul 23];21(6):453–60. Available from: https://pubmed.ncbi.nlm.nih.gov/30009705/.

[114] Boadu A, Agoni C, Karpoormath R, Soliman M, Nlooto M. Repurposing antiviral phytochemicals from the leaf extracts of Spondias mombin (Linn) towards the identification of potential SARSCOV-2 inhibitors. Sci Rep 2022;121 [Internet]. 2022 Jun 28 [cited 2023 Jul 22];12(1):1–14. Available from: https://www.nature.com/articles/s41598-022-14558-3.

[115] Rudrapal M, Eltayeb WA, Rakshit G, El-Arabey AA, Khan J, Aldosari SM, et al. Dual synergistic inhibition of COX and LOX by potential chemicals from Indian daily spices investigated through detailed computational studies. Sci Rep 2023;131 [Internet]. 2023 May 27 [cited 2023 Jul 31];13(1):1–27. Available from: https://www.nature.com/articles/s41598-023-35161-0.

[116] Daina A, Michielin O, Zoete V. SwissADME: A free web tool to evaluate pharmacokinetics, drug-likeness and medicinal chemistry friendliness of small molecules. Sci Rep 2017;7:1–13. October 2016.

[117] Drwal MN, Banerjee P, Dunkel M, Wettig MR, Preissner R. ProTox: A web server for the in silico prediction of rodent oral toxicity. Nucleic Acids Res 2014;42(W1):53–8.

[118] Filimonov DA, Lagunin AA, Gloriozova TA, Rudik AV, Druzhilovskii DS, Pogodin PV, et al. Prediction of the Biological Activity Spectra of Organic Compounds Using the Pass Online Web Resource. Chem Heterocycl Compd 2014;503 [Internet]. 2014 May 28 [cited 2022 Sep 19];50(3):444–57. Available from: https://link.springer.com/article/10.1007/s10593-014-1496-1.

[119] Monaghan P, Leneghan DB, Shaw W, Bell A. The antimalarial action of FK506 and rapamycin: evidence for a direct effect on FK506-binding protein PfFKBP35. 2017/03/09 Parasitology 2017;144(7):869–76.

[120] Monaghan P, Fardis M, Revill WP, Bell A. Antimalarial effects of macrolactones related to FK520 (ascomycin) are independent of the immunosuppressive properties of the compounds. J Infect Dis 2005 Apr;191(8):1342–9.

[121] Monaghan P, Bell A. A Plasmodium falciparum FK506-binding protein (FKBP) with peptidyl–prolyl cis–trans isomerase and chaperone activities. Mol Biochem Parasitol 2005;139(2):185–95.

[122] Bell A, Monaghan P, Page AP. Peptidyl-prolyl cis–trans isomerases (immunophilins) and their roles in parasite biochemistry, host–parasite interaction and antiparasitic drug action. Int J Parasitol 2006;36(3):261–76.

[123] Titov DV, Liu JO. Identification and validation of protein targets of bioactive small molecules. Bioorg Med Chem 2012 Mar;20(6):1902–9.

[124] Buckley DL, Crews CM. Small-molecule control of intracellular protein levels through modulation of the ubiquitin proteasome system. Angew Chem Int Ed Engl 2014 Feb;53(9):2312–30.

[125] Issahaku AR, Mukelabai N, Agoni C, Rudrapal M, Aldosari SM, Almalki SG, et al. Characterization of the binding of MRTX1133 as an avenue for the discovery of potential KRASG12D inhibitors for cancer therapy. Sci Rep 2022;12(1):17796.

[126] Issahaku AR, Agoni C, Kumi RO, Olotu FA, Soliman MES. Lipid-Embedded Molecular Dynamics Simulation Model for Exploring the Reverse Prostaglandin D2 Agonism of CT-133 towards CRTH2 in the Treatment of Type-2 Inflammation Dependent Diseases. Chem Biodivers 2020 Mar;17(3):e1900548.

[127] Agoni C, Issahaku AR, Abdelgawad MA, Khames A, Soliman MES, Mathew B. Extended Double Bond Conjugation in the Chalcone Framework Favours MAO-B Inhibition: A Structural Perspective on Molecular Dynamics. Comb Chem High Throughput Screen 2022 Feb 14;25(12):2059–69.

[128] Guterres H, Im W. Improving Protein-Ligand Docking Results with High-Throughput Molecular Dynamics Simulations. J Chem Inf Model 2020 Apr;60(4):2189–98.

[129] Liu K, Watanabe E, Kokubo H. Exploring the stability of ligand binding modes to proteins by molecular dynamics simulations. J Comput Aided Mol Des 2017;31(2):201–11.

[130] Scanu S, Foerster JM, Timmer M, Ullmann GM, Ubbink M. Loss of electrostatic interactions causes increase of dynamics within the plastocyanin-cytochrome f complex. Biochemistry 2013;52(38):6615–26.

[131] Li Y, Han L, Liu Z, Wang R. Comparative assessment of scoring functions on an updated benchmark: 2. Evaluation methods and general results. J Chem Inf Model 2014 Jun;54(6):1717–36.

[132] Jones G, Willett P, Glen RC, Leach AR, Taylor R. Development and validation of a genetic algorithm for flexible docking. J Mol Biol 1997;267(3):727–48.

[133] Santos LHS, Ferreira RS, Caffarena ER. Integrating Molecular Docking and Molecular Dynamics Simulations. Methods Mol Biol 2019;2053:13–34.

[134] Ali SA, Hassan MI, Islam A, Ahmad F. A review of methods available to estimate solvent-accessible surface areas of soluble proteins in the folded and unfolded states. Curr Protein Pept Sci 2014;15(5):456–76.

[135] Williams MA. Protein-ligand interactions: fundamentals. Methods Mol Biol 2013; 1008:3–34.

[136] Agha KA, Abo-Dya NE, Issahaku AR, Agoni C, Soliman MES, Abdel-Aal EH, et al. Novel Sunifiram-carbamate hybrids as potential dual acetylcholinesterase inhibitor and NMDAR co-agonist: simulation-guided analogue design and pharmacological screening. J Enzym Inhib Med Chem 2022 Dec;37(1):1241–56.

[137] Cooper GM. Signaling molecules and their receptors. 2000.

[138] Hao GF, Xu WF, Yang SG, Yang GF. Multiple simulated annealing-molecular dynamics (MSA-MD) for conformational space search of peptide and miniprotein. Sci Rep 2015;5(October):1–10.

[139] Kapla J, Espigares IR, Ballante F, Selent J, Carlsson J. Can molecular dynamics simulations improve the structural accuracy and virtual screening performance of GPCR models? PLoS Comput Biol 2021;17:1–33.

[140] Smith RD, Carlson HA. Identification of Cryptic Binding Sites Using MixMD with Standard and Accelerated Molecular Dynamics. J Chem Inf Model 2021 Mar;61 (3):1287–99.

[141] Oluyemi WM, Samuel BB, Adewumi AT, Adekunle YA, Soliman MES, Krenn L. An allosteric inhibitory potential of triterpenes from combretum racemosum on the structural and functional dynamics of plasmodium falciparum lactate dehydrogenase binding landscape [Internet] Chem Biodivers 2022 Feb 1 [cited 2023 May 16];19(2):e202100646. Available from: https://onlinelibrary.wiley.co m/doi/full/10.1002/cbdv.202100646.

[142] Miller 3rd BR, McGee TDJ, Swails JM, Homeyer N, Gohlke H, Roitberg AE. MMPBSA.py: An Efficient Program for End-State Free Energy Calculations. J Chem Theor Comput 2012 Sep;8(9):3314–21.

[143] Issahaku AR, Aljoundi A, Soliman MES. Establishing the mutational effect on the binding susceptibility of AMG510 to KRAS switch II binding pocket: Computational insights. Inform Med Unlocked 2022;30:100952.

[144] Pantsar T, Poso A. Binding Affinity via Docking: Fact and Fiction. Molecules 2018 Jul;23(8).

[145] Dahlin JL, Inglese J, Walters MA. Mitigating risk in academic preclinical drug discovery. Nat Rev Drug Discov 2015 Apr;14(4):279–94.

[146] Cheng F, Li W, Zhou Y, Shen J, Wu Z, Liu G, et al. admetSAR: a comprehensive source and free tool for assessment of chemical ADMET properties. J Chem Inf Model 2012 Nov;52(11):3099–105.

[147] Lipinski CA, Lombardo F, Dominy BW, Feeney PJ. Experimental and computational approaches to estimate solubility and permeability in drug discovery and development setting. Adv Drug Deliv Rev 2012;64:4–17.

[148] Daina A, Zoete V. A BOILED-Egg To Predict Gastrointestinal Absorption and Brain Penetration of Small Molecules. ChemMedChem 2016:1117–21.

[149] Johnson TW, Gallego RA, Edwards MP. Lipophilic Efficiency as an Important Metric in Drug Design. J Med Chem 2018 Aug;61(15):6401–20.

[150] Struck S, Schmidt U, Gruening B, Jaeger I, Hossbach J, Preissner R. Toxicity versus potency: elucidation of toxicity properties discriminating between toxins, drugs, and natural compounds. Genome Inf 2008;20:231–42.

[151] Ertl P, Rohde B, Selzer P. Fast calculation of molecular polar surface area as a sum of fragment-based contributions and its application to the prediction of drug transport properties. J Med Chem 2000 Oct;43(20):3714–7.

[152] Prasanna S, Doerksen RJ. Topological polar surface area: a useful descriptor in 2D-QSAR. Curr Med Chem 2009;16(1):21–41.

[153] Shityakov S, Neuhaus W, Dandekar T, Forster C. Analysing molecular polar surface descriptors to predict blood-brain barrier permeation. Int J Comput Biol Drug Des 2013;6:146–56.

[154] Morris-Schaffer K, McCoy MJ. A Review of the LD50 and Its Current Role in Hazard Communication. ACS Chem Heal Saf 2021 Jan;28(1):25–33.

[155] Mehanna WE, Lu T, Debnath B, Lasheen DS, Serya RAT, Abouzid KA, et al. Synthesis, ADMET Properties, and Biological Evaluation of Benzothiazole Compounds Targeting Chemokine Receptor 2 (CXCR2). ChemMedChem 2017 Jul; 12(13):1045–54.

[156] Goel RK, Singh D, Lagunin A, Poroikov V. PASS-assisted exploration of new therapeutic potential of natural products. Med Chem Res 2010;209 [Internet]. 2010 Aug 6 [cited 2022 Sep 20];20(9):1509–14. Available from: https://link.spri nger.com/article/10.1007/s00044-010-9398-y.

[157] Thurston S, Hite GL, Petry AN, Ray SD. Antiprotozoal Drugs 2015:321–7.

[158] Clements RL, Streva V, Dumoulin P, Huang W, Owens E, Raj DK, et al. A Novel Antiparasitic Compound Kills Ring-Stage Plasmodium falciparum and Retains Activity Against Artemisinin-Resistant Parasites. J Infect Dis 2020 Mar;221(6): 956–62.